inorganics

MDPI

Article

Comparative Solution Equilibrium Studies on Anticancer Estradiol-Based Conjugates and Their Copper Complexes

Éva A. Enyedy [1,2,*], Anett Giricz [1,2], Tatsiana V. Petrasheuskaya [1,2], János P. Mészáros [1,2], Nóra V. May [3], Gabriella Spengler [1,4], Ferenc Kovács [2], Barnabás Molnár [2] and Éva Frank [2]

1 MTA-SZTE Lendület Functional Metal Complexes Research Group, University of Szeged, Dóm Tér 7-8, H-6720 Szeged, Hungary; petrashevtanya@chem.u-szeged.hu (T.V.P.); meszaros.janos@chem.u-szeged.hu (J.P.M.); spengler.gabriella@med.u-szeged.hu (G.S.)
2 Department of Molecular and Analytical Chemistry, Interdisciplinary Excellence Centre, University of Szeged, Dóm Tér 7-8, H-6720 Szeged, Hungary; ferenc.kovacs@chem.u-szeged.hu (F.K.); barnabas.molnar@chem.u-szeged.hu (B.M.); frank@chem.u-szeged.hu (É.F.)
3 Centre for Structural Science, HUN-REN Research Centre for Natural Sciences, Magyar Tudósok Körútja 2, H-1117 Budapest, Hungary; may.nora@ttk.hu
4 Department of Medical Microbiology, Albert Szent-Györgyi Health Center, Albert Szent-Györgyi Medical School, University of Szeged, Semmelweis U. 6, H-6725 Szeged, Hungary
* Correspondence: enyedy@chem.u-szeged.hu

Abstract: Steroids are often considered valuable molecular tools for the development of anticancer agents with improved pharmacological properties. Conjugation of metal chelating moieties with a lipophilic sterane backbone is a viable option to obtain novel anticancer compounds. In this work, two estradiol-based hybrid molecules (PMA-E2 and DMA-E2) with an (*N*,*N*,*O*) binding motif and their Cu(II) complexes were developed. The lipophilicity, solubility, and acid-base properties of the novel ligands were determined by the combined use of UV-visible spectrophotometry, pH-potentiometry, and ^{1}H NMR spectroscopy. The solution speciation and redox activity of the Cu(II) complexes were also investigated by means of UV-visible and electron paramagnetic resonance spectroscopy. Two structurally analogous ligands (PMAP and DMAP) were also included in the studies for better interpretation of the solution chemical data obtained. Three pK_a values were determined for all ligands, revealing the order of the deprotonation steps: pyridinium-NH^+ or $NH(CH_3)_2^+$, secondary NH_2^+, and OH. The dimethylamine derivatives (DMA-E2, DMAP) are found in their H_2L^+ forms in solution at pH 7.4, whereas the fraction of the neutral HL species is significant (34–37%) in the case of the pyridine nitrogen-containing derivatives (PMA-E2, PMAP). Both estradiol derivatives were moderately cytotoxic in human breast (MCF-7) and colon adenocarcinoma (Colo-205) cells (IC_{50} = 30–63 μM). They form highly stable complexes with Cu(II) ions capable of oxidizing ascorbate and glutathione. These Cu(II) complexes are somewhat more cytotoxic (IC_{50} = 15–45 μM) than their corresponding ligands and show a better selectivity profile.

Keywords: estradiol hybrids; stability constants; chelators; solution speciation; cytotoxicity

Citation: Enyedy, É.A.; Giricz, A.; Petrasheuskaya, T.V.; Mészáros, J.P.; May, N.V.; Spengler, G.; Kovács, F.; Molnár, B.; Frank, É. Comparative Solution Equilibrium Studies on Anticancer Estradiol-Based Conjugates and Their Copper Complexes. *Inorganics* **2024**, *12*, 49. https://doi.org/10.3390/inorganics12020049

Academic Editors: Tamara Topala, Luminita Simona Oprean and Andreea Elena Bodoki

Received: 30 December 2023
Revised: 26 January 2024
Accepted: 29 January 2024
Published: 1 February 2024

1. Introduction

The potential use of steroids in chemotherapy has been investigated for decades, and some compounds, such as abiraterone and fulvestrant, have been successfully introduced into routine clinical practice for the treatment of prostate and breast cancer, respectively [1,2]. Consequently, the sterane skeleton has become a valuable structural motif in the development of innovative anticancer agents. Molecular hybridization, in which two pharmacophores are incorporated into the same molecule, has emerged as a promising strategy; therefore, conjugation of the steroid scaffold with other anticancer agents may lead to novel compounds with enhanced anticancer activity, altered mechanisms of action, and the ability to reduce side effects and overcome drug resistance [3–5].

The combination of a metal chelating ligand with a lipophilic sterane backbone has proven to be a preferred approach, as exemplified by our previous works on salicylhydroxamic acid and thiosemicarbazone derivatives (Chart 1) [6–10]. These estrone (E1) or estradiol (E2) conjugates are substituted at position 2 of the A-ring based on the finding that this type of substitution results in negligible binding to estrogen receptors [2,5,11]. Comprehensive reviews of metallodrug conjugates with steroids have been provided by Biersack et al. [12] and Bideau et al. [13]. Furthermore, numerous examples of Pt(II) [14–21], organoruthenium [22–24], and Cu(II) [25,26] complexes with a steroidal backbone as a pharmacophore have been reported.

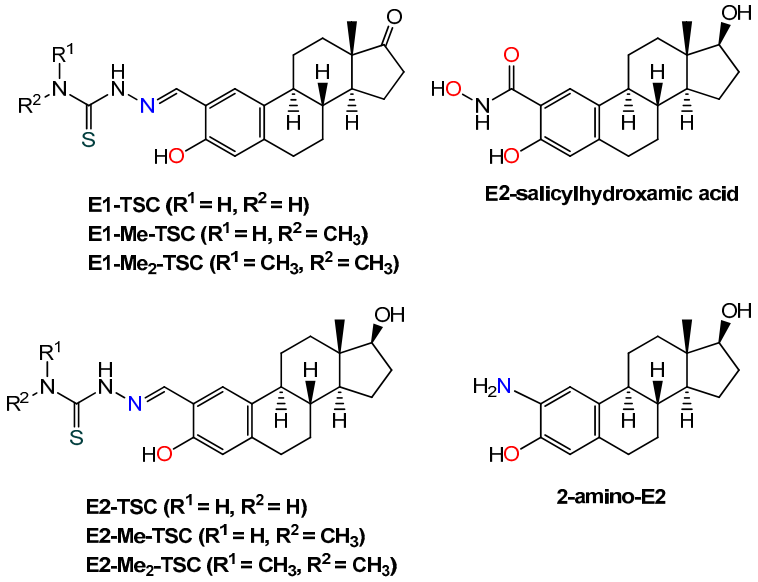

Chart 1. Chemical structures of previously studied estrone- (E1) and estradiol- (E2) thiosemicarbazone (TSC) and salicylhydroxamic acid hybrids in addition to 2-aminoestradiol [6–10].

The estradiol-salicylhydroxamic acid hybrid, bearing the (*O*,*O*) donor set, showed moderate anticancer activity (IC_{50} = 25–59 μM) in human cancer cell lines (Colo-205, Colo-320, MCF-7) and displayed a favorable selectivity profile, being non-toxic in non-cancerous MRC-5 cells [9]. Moreover, its organometallic half-sandwich Rh(III)(η^5-$C_5(CH_3)_5$) and Ru(II)(η^6-*p*-cymene) complexes exhibited slightly improved activity [9] compared to the ligand alone [9]. In the case of the thiosemicarbazone derivatives with the (*S*,*N*,*O*) donor set, the in vitro cytotoxic activity was increased upon the conjugation, which was further enhanced by complex formation with Cu(II) ions [6–8]. The Cu(II) complexes of terminal *N*-mono- and dimethylated estrone-salicylaldehyde thiosemicarbazone derivatives displayed low IC_{50} values (3.9–17.1 μM) in different 3D spheroids of human cancer cells (HCT-116, A-549, CH-1), induced significant morphological changes and tumor shrinkage, and activated caspase-3 and caspase-7 endoproteases, leading to apoptosis [7].

The effect of the domain-integrated hybridization of 2-aminophenol with estradiol on cytotoxicity and solution chemical properties was also investigated. 2-Aminoestradiol (2-amino-E2, Chart 1) displayed high cytotoxicity in HeLa, Colo-205, and the doxorubicin-resistant Colo-320 cell lines, whereas 2-aminophenol and estradiol alone were not toxic in these cancer cells [10]. The complex formation with Cu(II) ions resulted in elevated cytotoxicity in MCF-7 breast cancer cells and a higher percentage of apoptotic cells. It is noteworthy that this derivative was less sensitive to oxidation than the reference compound, 2-aminophenol.

In this work, 2-aminomethylestradiol derivatives with increased denticity, namely by incorporating an additional *N*-donor at the chelatable position (PMA-E2 and DMA-E2, Chart 2), yielding compounds with a (*N*,*N*,*O*) donor set, have been developed. For comparative purposes, the solution chemical properties, including Cu(II) binding ability, of their non-steroidal models (PMAP and DMAP, Chart 2) were also investigated.

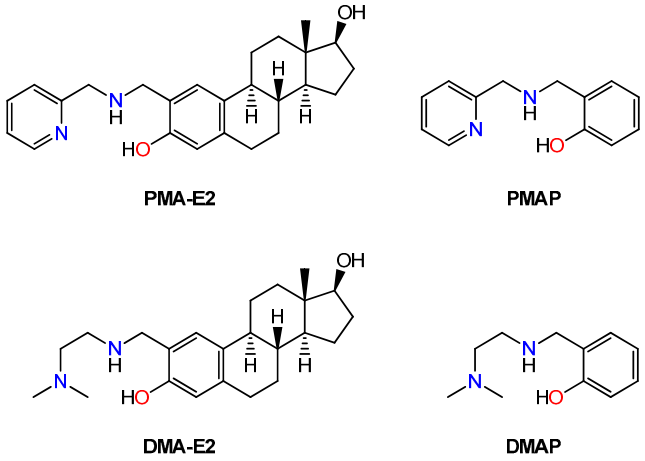

Chart 2. Chemical structures of 2-((((2-pyridin-2-yl)methyl)amino)methyl)estradiol (PMA-E2), 2-(((2-(dimethylamino)ethyl)amino)methyl)estradiol (DMA-E2), 2-((((pyridin-2-yl)methyl)amino) methyl)phenol (PMAP), and 2-(((2-(dimethylamino)ethyl)amino)methyl)phenol (DMAP) in their neutral forms (HL).

The mono-ligand Cu(II) complex of the pyridine-N-containing PMAP was previously tested in both in vitro and in vivo assays. This complex showed only moderate cytotoxicity in human THP-1 leukemia and Colo-205 cancer cells, but it could significantly suppress the growth of THP-1 monocytic sarcoma in mice [27]. Based on the X-ray crystallography data reported in this work, the complex contained the neutral ligand coordinated via the amine and pyridine N-atoms and the protonated phenol oxygen, while the coordination sphere was saturated by two chlorido ligands [27]. The structure of the bis-ligand complex was also reported, for which the 2 × (*N*,*N*,*OH*) coordination mode was found in the solid phase [28]. The Cu(II) complex of PMAP was found to bind to DNA and to exhibit DNA cleavage activity [29]. Based on these results, we have concluded that PMAP is worth conjugating to the sterane scaffold. Despite the lack of reported cytotoxicity data for DMAP or its Cu(II) complexes, we aimed to investigate the effect of replacing the pyridine with an aliphatic amine nitrogen on the complexing ability and bioactivity.

Therefore, we report here the synthesis and characterization of two tridentate estradiol derivatives (PMA-E2, DMA-E2) and their Cu(II) complexes. The solution behavior of these ligands and their model compounds was investigated by pH-potentiometric, UV-visible (UV-vis), and ^{1}H NMR spectroscopic titrations. The solution stability and structure of their Cu(II) complexes were studied by pH-potentiometric and UV-vis titrations, and electron paramagnetic resonance (EPR) spectroscopy was also employed. Meanwhile, the redox properties of the Cu(II) complexes were assayed by cyclic voltammetry, and their direct reactions with the natural reducing agents glutathione (GSH) and ascorbic acid were also monitored. The anticancer activity of the estradiol hybrids and their Cu(II) complexes was tested in human MCF-7 breast and Colo-205 colon adenocarcinoma cell lines.

2. Results and Discussion

2.1. Synthesis and Characterization of PMA-E2, DMA-E2 and Their Model Compounds (PMAP, DMAP)

The novel tridentate steroidal ligands (PMA-E2 and DMA-E2) were prepared from 2-formylestrone (F-E1) [30] and the appropriate amine reagent (2-picolylamine or *N*,*N*-dimethylethylenediamine) via reductive amination (Scheme 1). Under the conditions used, stereoselective reduction of the C17-ketone also occurred, resulting in estradiol (E2) derivatives. For the similar synthesis of non-steroidal model compounds (PMAP and DMAP), which correspond to the A ring of their sterane analogs, salicylic aldehyde was applied as the starting material. The corresponding amines [31,32] were obtained in moderate yields. The products were characterized by ^{1}H and ^{13}C NMR spectroscopy

(Figures S1–S8), and the spectra were in agreement with the proposed structures, enabling the assignment of all resonances.

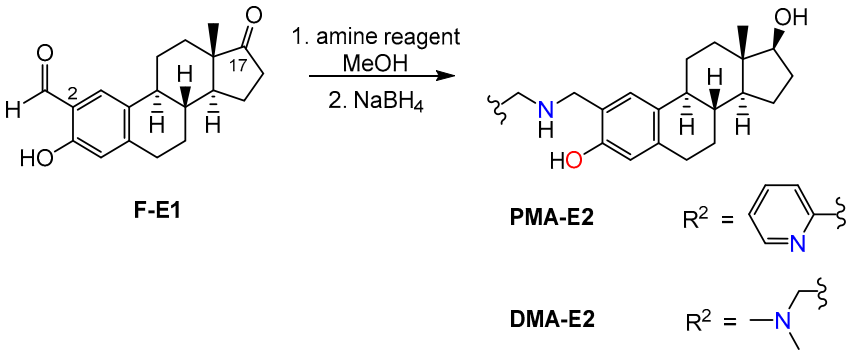

Scheme 1. Synthesis of novel steroidal tridentate ligands by reductive amination of 2-formylestrone (F-E1). Amine reagent: 2-picolylamine (for PMA-E2) or *N*,*N*-dimethylethylenediamine (for DMA-E2) (Other abbreviation: MeOH = methanol).

2.2. Solution Chemical Properties of PMA-E2, DMA-E2, and the Model Ligands PMAP and DMAP

Sterane-based compounds often exhibit restricted aqueous solubility. Consequently, prior to the solution equilibrium studies, the thermodynamic aqueous solubility ($S_{7.4}$) and the lipophilicity of PMA-E2 and DMA-E2 (Chart 2) were characterized at pH 7.4 using UV-vis spectrophotometry for the analysis. The obtained values of $S_{7.4}$ = 230 ± 10 μM for PMA-E2 and 2.7 ± 0.1 mM for DMA-E2 reflect the much better solubility of the latter compound bearing the tertiary ammonium group. The distribution coefficients ($D_{7.4}$) were determined via traditional n-octanol-H_2O partitioning in the presence of 0.1 M KCl. The obtained $logD_{7.4}$ values of +0.5 ± 0.1 for PMA-E2 and +1.8 ± 0.1 for DMA-E2 reveal moderate and high lipophilicity, respectively. It is noteworthy that DMA-E2 exhibits a lipophilic characteristic despite its favorable aqueous solubility. Presumably, the protonated form of DMA-E2 with a counter-chloride ion undergoes transfer to the apolar phase. Thus, a 30% (*v*/*v*) DMSO/H_2O solvent mixture was selected for the solution equilibrium studies to provide the required solubility, and this particular solvent medium was also employed in our previous works involving sterane-based ligands [6–10]. For the measurements, the stock solutions of the compounds were prepared in DMSO, and their long-term stability in solution was tracked by ^{1}H NMR spectroscopy. According to the spectra presented in Figure S9, all the studied compounds (PMA-E2, DMA-E2, PMAP, and DMAP) maintained stability throughout the 6-day monitoring period.

First, UV-vis spectrophotometric titrations were performed to determine the proton dissociation constants (pK_a) for PMA-E2 and DMA-E2 (Table 1). The fully protonated forms of these compounds (H_3L^{2+}) possess three dissociable protons, and correspondingly, the spectral changes (as illustrated for PMA-E2 in Figure 1) indicated three deprotonation processes. (It is worth noting that the hydroxyl group on the D-ring of the sterane ring system has a pK_a value so high that it is not considered to be dissociable in the studied pH range). However, in the case of PMA-E2, the first deprotonation occurs at fairly acidic pH values, which hindered the determination of the pK_1 value. Whereas, the second step occurring within the neutral pH range was characterized by only minor spectral changes, leading to a degree of uncertainty in the obtained value. The third process in the basic pH range resulted in significant spectral changes, and an increase in the λ_{max} was seen, which often originated from a more extended conjugated π-electron system of the deprotonated form. This phenomenon is typically observed for the deprotonation of phenolic OH groups.

Table 1. pK_a values of the ligands determined by pH-potentiometry (pH-pot.) and UV-vis spectrophotometric titrations in 30% (v/v) DMSO/H_2O. HL is the neutral form of the ligands (Scheme 1). {T = 25 °C, I = 0.10 M (KCl)}.

Method	Constant	PMA-E2	DMA-E2	PMAP	DMAP
UV-vis	pK_1 (H_3L^{2+})	<1.5	5.77 ± 0.07	<1.5	5.69 ± 0.03
	pK_2 (H_2L^{+})	~7.6	8.81 ± 0.03	7.62 ± 0.03	8.68 ± 0.04
	pK_3 (HL)	11.21 ± 0.08	11.26 ± 0.03	10.78 ± 0.03	10.90 ± 0.05
pH-pot.	pK_1 (H_3L^{2+})	<1.5	5.88 ± 0.06	<1.5	5.81 ± 0.07
	pK_2 (H_2L^{+})	7.69 ± 0.06	8.99 ± 0.04	7.62 ± 0.03	8.69 ± 0.05
	pK_3 (HL)	11.01 ± 0.04	11.19 ± 0.03	10.69 ± 0.03	10.85 ± 0.04

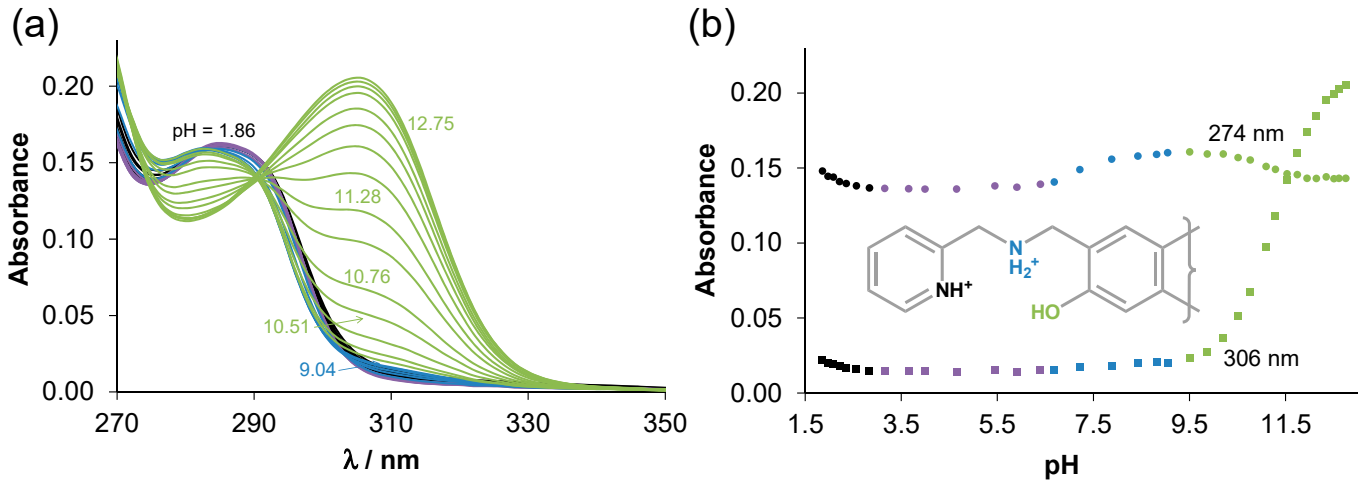

Figure 1. (**a**) UV-vis absorption spectra of PMA-E2 recorded at different pH values in 30% (v/v) DMSO/H_2O and (**b**) absorbance values measured at 274 nm (●) and 306 nm (■) with the fully protonated form of the ligand. The assigned color codes serve to indicate the deprotonating moieties within the given pH range. {c_{ligand} = 50 μM; T = 25 °C; I = 0.10 M (KCl); ℓ = 1 cm}.

For DMA-E2, three pK_a values could be computed, although only the third process resulted in greater changes in the spectra resembling those observed for PMA-E2. We also attempted to conduct pH-potentiometric titrations in 30% (v/v) DMSO/H_2O using low concentrations (0.5 mM) due to the limited solubility. (Upon the deprotonation of DMA-E2, the solubility decreased). No precipitate was observed; however, achieving more reliable data would have required higher concentrations. Nevertheless, the pK_a values obtained from the two different methods are in good agreement (Table 1).

To validate the reliability of the acidity constants of the estradiol derivatives, pK_a values for the structurally analogous ligands (PMAP and DMAP, Chart 2) with increased aqueous solubility were also determined using both methods (Table 1). These model ligands displayed the same deprotonation pattern as the sterane-based compounds, and the corresponding pK_1 values were also quite alike. However, the pK_2 constants of DMAP obtained by both methods were somewhat lower than those of DMA-E2, and the pK_3 constants of PMAP and DMAP were significantly lower than those of PMA-E2 and DMA-E2, respectively. Based on the observed spectral changes, pK_3 is assigned to the phenolic-OH moiety, and its value is increased for the estradiol derivatives as a consequence of the electron-donating effect of the sterane scaffold.

In the case of PMAP as well as PMA-E2, the difference between the pK_a values reflects well-separated dissociation steps in the order of pyridinium-NH^+, secondary NH_2^+, and OH. Based on chemical evidence, it is apparent that the tertiary ammonium group in DMAP and DMA-E2 dissociates at a lower pH compared to the secondary ammonium nitrogen. Consequently, it is assumed that pK_1 of these compounds corresponds to the $NH(CH_3)_2^+$ moiety, while pK_2 does to the NH_2^+ group. Since the tertiary ammonium

group is situated at a considerable distance from the chromophoric unit, ^{1}H NMR titrations were performed to confirm the assignment of the pK_1 in the pH range of 2.20 to 8.50 in 30% (v/v) DMSO-d_6/H_2O for DMAP (Figure 2). The recorded spectra (Figure 2a) reveal that the peaks corresponding to the aromatic protons are slightly upfield shifted at pH exceeding ~5.5. The decrease in the chemical shifts of these protons is relatively small (Figure 2c), compared to the shifts observed for other peaks, as these protons are not so sensitive to the proton dissociation processes occurring within the monitored pH range. As it was expected, the signals of the protons nearby the tertiary nitrogen exhibit greater changes, already at pH > 4.5; however, the CH_2 protons located between the secondary nitrogen and the phenol ring also displayed sensitivity.

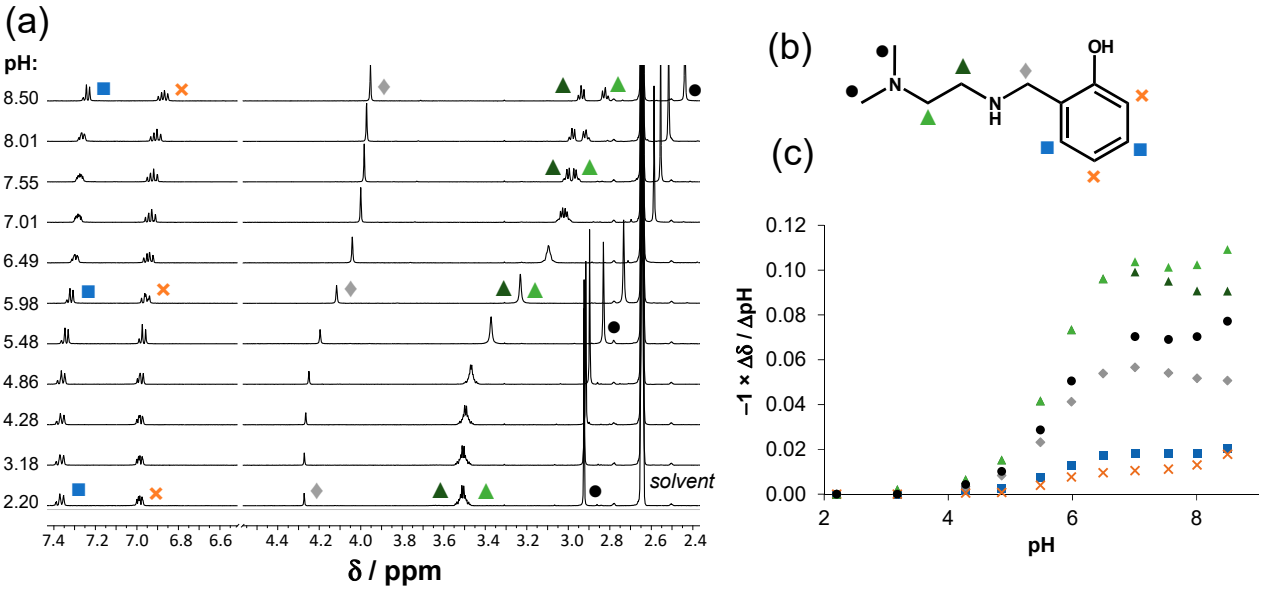

Figure 2. (**a**) ^{1}H NMR spectra of DMAP in 30% (v/v) DMSO-d_6/H_2O at the indicated pH values; (**b**) the structure of the ligands with the notation of the symbols of the carbon-bound protons; and (**c**) changes of the chemical shifts as the pH increased using the same symbols for the peaks of the specified protons in figure (**b**). {c_{ligand} = 1.0 mM; pH = 2.2–8.5; T = 25 °C; I = 0.10 M (KCl)}.

Using the obtained pK_a values, concentration distribution curves were computed (Figure 3), and it can be concluded that at pH 7.4, DMA-E2 and DMAP primarily exist in their H_2L^+ forms (95% and 93%, respectively), and only a smaller fraction is in the neutral HL form. Meanwhile, for the ligands containing a pyridine moiety, there is a greater fraction of the HL species (PMA-E2: 66% H_2L^+, 34% HL; and PMAP: 63% H_2L^+, 37% HL). Most probably, this feature also contributes to the lower aqueous solubility of PMA-E2 compared to DMA-E2.

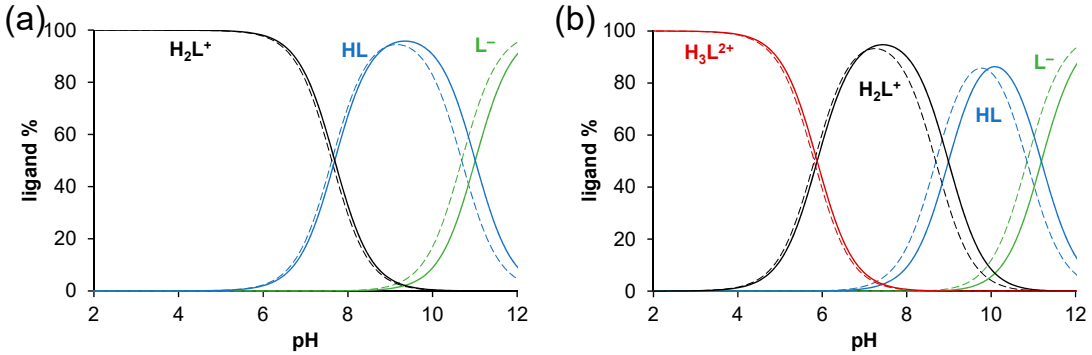

Figure 3. Concentration distribution curves for (**a**) PMA-E2 (solid lines) and PMAP (dashed lines), and (**b**) DMA-E2 (solid lines) and DMAP (dashed lines). {c_{ligand} = 50 μM; 30% (v/v) DMSO/H_2O; T = 25 °C; I = 0.10 M (KCl)}.

2.3. Complex Formation Equilibria of the Ligands with Cu(II) Ions in Solution

Interaction between the model compounds (PMAP and DMAP) and Cu(II) ions was studied by both pH-potentiometry and UV-vis spectrophotometry, and the calculated formation constants (β) are shown in Table 2. As the formation constants were determined in the presence of 30% (*v*/*v*) DMSO, they are only valid in this medium; in water, slightly different stability constants would be obtained. On the basis of the titration data obtained by both methods, the formation of only mono-ligand complexes $[CuL]^+$ and $[CuLH_{-1}]$ was observed even at higher metal-to-ligand ratios. It should be noted that in the mono and bis complexes characterized by X-ray crystallography, the coordination of the neutral ligand(s) with the protonated phenol group has been reported for PMAP [27–29], but these results are relevant for the solid phase. While the phenoxo-bridged dinuclear Cu(II) complexes with a 1:1 metal-to-ligand ratio were also shown for both PMAP and DMAP in the solid phase [33,34], a mixed-bridged (phenoxo and chlorido) trinuclear complex of PMAP was reported as well [35]. In the complex $[CuL]^+$ formed in the solution, the ligand coordinates in its deprotonated form, thus $[(N,N,O^-)(solvent)]$ binding mode is likely. The coordinated solvent is not denoted in the simple formula of the species. It is noteworthy that both DMSO and H_2O molecules can act as co-ligands in the applied medium. This particular complex is characterized by λ_{max} values at 655 and 413 nm (as shown for DMAP in Figure 4a) and at 643 and 412 nm (for PMAP, not shown). The pK_a value of $[CuL]^+$ for both PMAP and DMAP (Table 2) is ca. 10.

Table 2. Overall stability constants (β) of the Cu(II) complexes formed with the ligands determined by UV-vis spectrophotometry and pH-potentiometry in 30% (*v*/*v*) DMSO/H_2O, pK_a of the species $[CuL]^+$ and pCu values at pH 7.4. {T = 25 °C, I = 0.10 M (KCl)}.

Constant	Method	PMA-E2	DMA-E2	PMAP	DMAP
logβ $[CuL]^+$	UV-vis	15.15 ± 0.03	15.58 ± 0.03	14.94 ± 0.03	15.30 ± 0.03
	pH-pot.	-	-	15.06 ± 0.09	15.38 ± 0.06
logβ $[CuLH_{-1}]$	UV-vis	4.96 ± 0.03	5.63 ± 0.03	4.80 ± 0.03	5.30 ± 0.03
	pH-pot.	-	-	5.13 ± 0.09	5.48 ± 0.08
pK_a $[CuL]^+$	UV-vis	10.19	9.95	10.14	10.00
	pH-pot.	-	-	9.93	9.90
pCu [a]		8.1	7.7	8.3	7.8

[a] pCu = −log[Cu(II)] computed at pH = 7.4, $c_{ligand} = c_{Cu(II)}$ = 10 µM; 30% (*v*/*v*) DMSO/H_2O; T = 25 °C; I = 0.10 M (KCl).

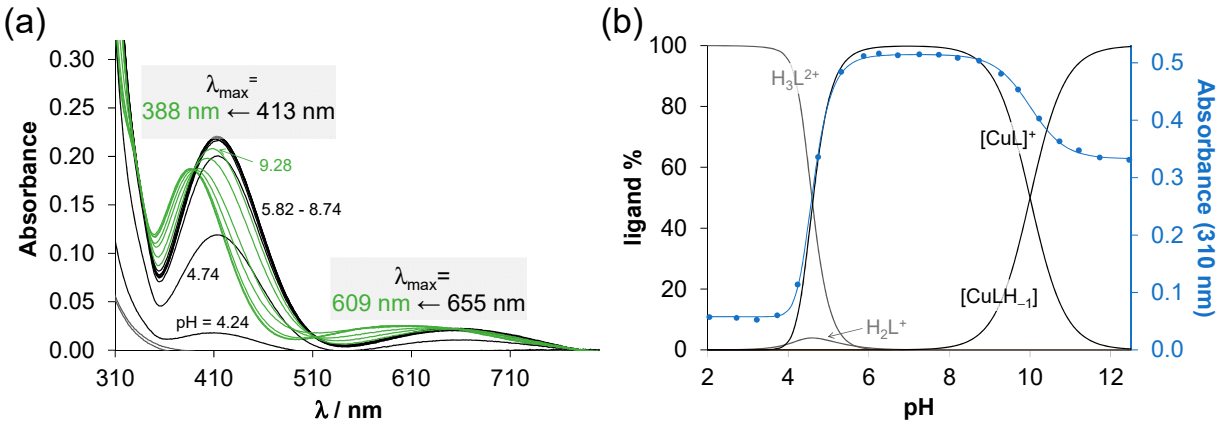

Figure 4. (**a**) UV-vis absorption spectra recorded for the Cu(II)—DMAP (1:1) system at different pH values. (**b**) Concentration distribution curves calculated under the same conditions with absorbance values measured at 310 nm (•). {$c_{ligand} = c_{Cu(II)}$ = 276 µM; 30% (*v*/*v*) DMSO/H_2O; T = 25 °C; I = 0.10 M (KCl); ℓ = 1 cm}.

This may suggest the deprotonation of the aqua ligand, leading to the formation of a mixed hydroxido species [CuL(OH)]. Alternatively, another possibility arises, where the

coordinated ligand may further deprotonate at the secondary N, resulting in the complex [CuLH$_{-1}$] with an [(*N*,*N*$^-$,*O*$^-$)(solvent)] binding mode. The notable shifts in the λ_{max} values towards the lower wavelengths in the basic pH range (PMAP: 655 nm → 609 nm, 413 nm → 388 nm (Figure 4a), DMAP: 643 nm → 588 nm, and 412 nm → 386 nm, not shown) indicate a preference for ligand binding via the (*N*,*N*$^-$,*O*$^-$) donor set rather than the formation of the mixed hydroxido complex.

In the case of the Cu(II) complexes with the estradiol derivatives, only UV-vis titrations were conducted using a 50 μM ligand concentration due to the worse aqueous solubility of the Cu(II) complexes compared to the ligands, especially in the basic pH range. Based on the spectral data collected, the formation of [CuL]$^+$ and [CuLH$_{-1}$] were postulated, and their overall stability (formation) constants are seen in Table 2. Thus, the same speciation model and similar equilibrium constants were obtained for the corresponding model ligands. Concentration distribution curves computed with the formation constants for the Cu(II)—PMA-E2 and Cu(II)—PMAP systems (Figure 5a) clearly show this similarity. The formation of the [CuLH$_{-1}$] species was also accompanied in the basic pH range by the decrease in the λ_{max} values (PMA-E2: 428 nm → 400 nm, DMA-E2: 428 nm → 388 nm; the d-d bands appeared with too low absorbance due to the low concentrations applied). It also suggests the formation of [CuLH$_{-1}$] (instead of [CuL(OH)]) in the basic pH range, as the suggested coordination modes are shown in Figure 5b.

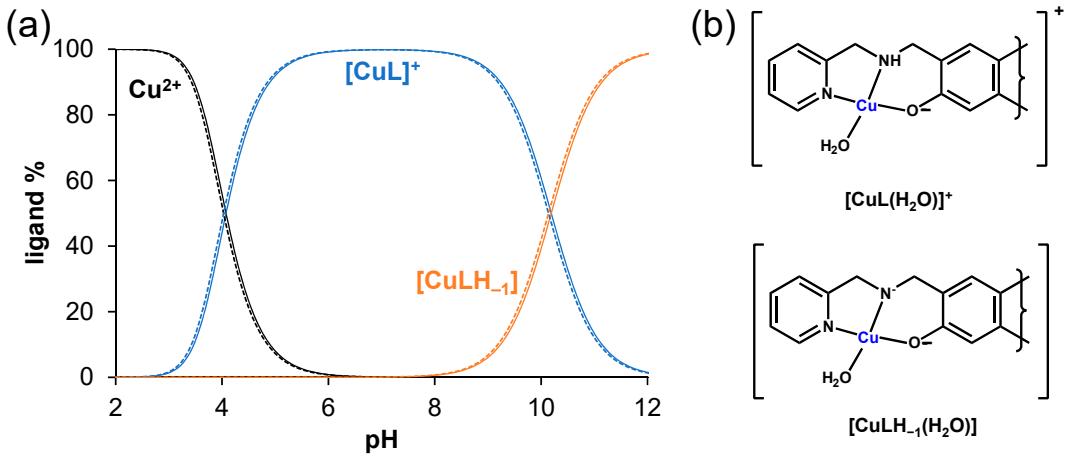

Figure 5. (**a**) Concentration distribution curves computed for the Cu(II)—PMA-E2 (1:1) (solid lines) and Cu(II)—PMAP (1:1) (dashed lines) systems. (**b**) Suggested coordination modes in the [CuL]$^+$ and [CuLH$_{-1}$] complexes. It should be noted that the H_2O co-ligand might be partly replaced by the DMSO co-solvent. {$c_{ligand} = c_{Cu(II)}$ = 50 μM; 30% (*v*/*v*) DMSO/H_2O; *T* = 25 °C; *I* = 0.10 M (KCl)}.

In order to confirm the coordination modes in the complexes and the speciation models, EPR spectroscopic measurements were performed. For this study, DMA-E2 was selected due to its better aqueous solubility compared to PMA-E2. EPR spectra could be recorded for its Cu(II) complexes at room temperature in a 30% (*v*/*v*) DMSO/H_2O solution at various pH values, and titrations were also performed for the model compound DMAP (Figure S10). A two-dimensional simulation of the solution EPR spectra resulted in the individual isotropic EPR spectra (Figure 6a,b) and parameters (Table 3).

Deconvolution of the EPR spectra using the overall stability constants of the complexes clearly shows the formation of two different types of complexes. The computed g_0 tensor and A_0 coupling constants are similar for the corresponding complexes of DMA-E2 and DMAP; however, significant differences were observed in the relaxation parameters. The higher α and lower β values of the DMA-E2 complexes indicate that the rotational averaging of the direction-dependent parameter is not complete in comparison to the complexes of the non-steroidal and less rigid model ligand. The complexes [CuLH$_{-1}$] were characterized in both cases by lower g_0 and slightly higher A_0 EPR parameters than those of [CuL]$^+$. Based on our previous reports, the formation of mixed hydroxido complexes

is often accompanied by narrowed lines and a better dissolved nitrogen structure [6–8], which also confirms that [CuLH$_{-1}$] is formed by the metal-induced deprotonation of the secondary nitrogen.

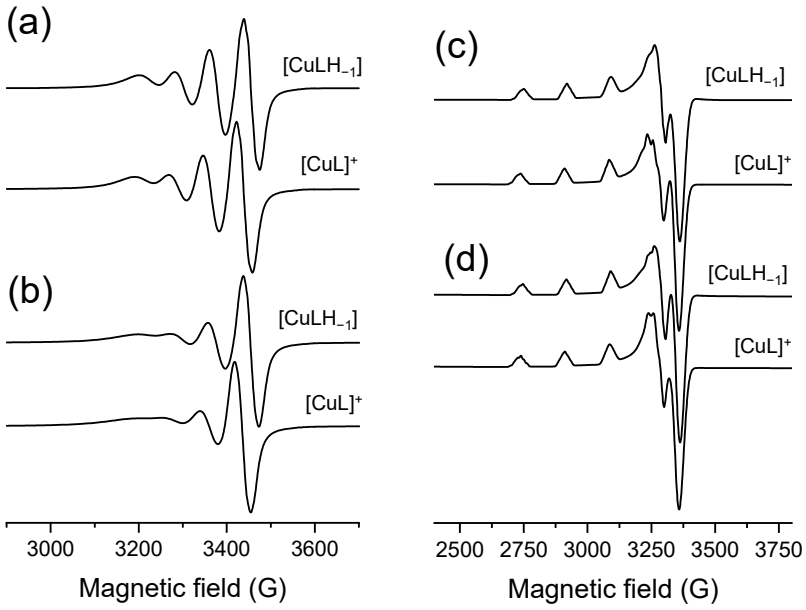

Figure 6. Calculated component EPR spectra at room temperature for (**a**) Cu(II)—DMAP and (**b**) Cu(II)—DMA-E2 complexes and at 77 K for (**c**) Cu(II)—DMAP and (**d**) Cu(II)—DMA-E2 complexes obtained by the simulation of pH-dependent EPR spectra. {30% (*v*/*v*) DMSO/H_2O; *I* = 0.10 M (KCl)}.

Table 3. EPR parameters [a] of the complexes determined from room temperature (isotropic) and at 77 K (anisotropic) EPR spectra recorded in Cu(II)—DMAP and Cu(II)—DMA-E2 equilibrium systems. {30% (*v*/*v*) DMSO/H_2O, *I* = 0.10 M (KCl)}.

	DMAP		**DMA-E2**	
	[CuL]$^{+}$	**[CuLH$_{-1}$]**	**[CuL]$^{+}$**	**[CuLH$_{-1}$]**
Isotropic Data				
g_0	2.116	2.108	2.117	2.108
A_0	70	72	69	72
a_0^N	10	10	10	10
α	27	24	46	39
β	−14	−13	−25	−21
γ	3	3	3	3
Anisotropic Data				
$g_\perp$	2.050	2.047	2.049	2.047
$g_\parallel$	2.248	2.242	2.248	2.244
$A_\perp$	24	23	21	24
$A_\parallel$	181	176	181	179
a_0^N	11	12	12	11
Calculated Data [b]				
$g_{0,calcd}$	2.116	2.112	2.116	2.113

[a] The coupling values are given in 10^{-4} cm^{-1}, the relaxation parameters are in G. The experimental error was ±0.001 for *g* and ±1 × 10^{-4} cm^{-1} for *A* parameters. [b] Calculated by the equation $g_0 = (2g_\perp + g_\parallel)/3$.

In addition to the measurement of the EPR spectra at room temperature, spectra were also recorded at 77 K (Figure S11). The anisotropic individual spectra are depicted in Figure 6c,d and the corresponding computed EPR parameters are also listed in Table 3. The anisotropic parameters are similar for the complexes formed with the estradiol derivative and the model ligand, whereas the differences between the g_0 tensor and A_0 coupling

constants of $[CuL]^+$ and $[CuLH_{-1}]$ are even smaller. Comparing the molar fractions of the complexes at specific pH values calculated for room temperature and the EPR anisotropic spectra (Figure S12), a discernible shift of complex formation and deprotonation processes towards higher pH values was detected at 77 K.

In order to compare the stability of the complexes of the studied ligands, pCu values were computed at pH 7.4 and at 10 μM concentrations of both the ligand and the metal ion using the formation constants (Table 2). pCu is defined as the negative decadic logarithm of the concentration of the free Cu(II) ions and serves as a solid basis for comparing the stability of the complexes under the given condition. The higher pCu value indicates a greater metal-binding capability of the ligand. The values are similar for the corresponding ligand pairs and higher for the compounds bearing a pyridine moiety. However, even in the case of the lowest pCu value (7.7), the dissociation of the complex is negligible (<1%).

In all, the studied ligands form highly stable Cu(II) complexes, and $[CuL]^+$ is the sole species at pH 7.4 in all cases, in which the ligands most likely coordinate in their monoanionic form through the (N,N,O^-) donor set.

2.4. Redox Properties of the Complexes Formed with Cu(II) Ions

Given that Cu(II) complexes often exert their pharmacological effect through their redox activity, and considering the high stability of the complexes formed with the studied tridentate ligands at physiological pH, as a first step, the redox properties of premixed complexes were investigated by cyclic voltammetry. Representative voltammograms for the Cu(II)—ligand systems are shown in Figure 7, and electrochemical data are collected in Table S1. Among the estradiol derivatives, only DMA-E2 could be assayed due to its better solubility. The voltammograms exhibited large peak separation (ΔE = 171–237 mV) (Figure 7a), and the quasi-reversible nature of the redox reaction became more pronounced with increasing scan rate (Figure 7b). The current measured in the Cu(II)—DMA-E2 system was plotted against the square root of the applied scan rate, and only in the case of the reduction peak it showed linearity, suggesting a diffusion-controlled electrode reaction (Figure 7b). The redox potentials ($E_{1/2}$) were similar for the complexes of the non-steroidal ligands (DMAP: −123 mV, PMAP: −155 mV vs. NHE), while a slightly lower value was obtained for the complex of DMA-E2 (−190 mV vs. NHE). These relatively low redox potentials reflect a weaker oxidizing power.

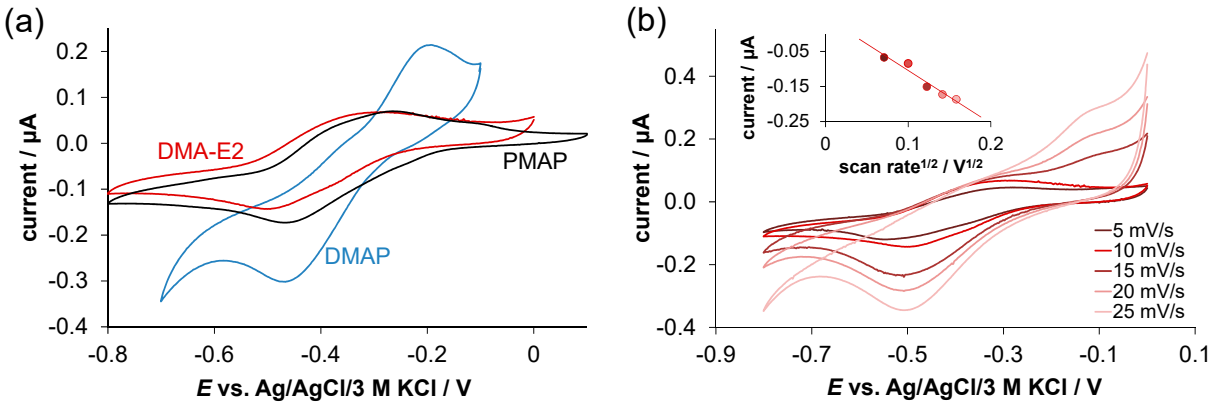

Figure 7. (**a**) Cyclic voltammograms of the Cu(II)—DMAP (blue line), Cu(II)—DMA-E2 (red line) and Cu(II)—PMAP (black line) systems at pH 7.4 using 10 mV/s scan rate. (**b**) Cyclic voltammograms of the Cu(II)—DMA-E2 system at pH 7.4 using various scan rates. Inserted figure shows the anodic peak current plotted against the square root of the scan rate. {30% (v/v) DMF/H_2O, c_{ligand} = 0.60 or 0.55 mM, $c_{Cu(II)}$ = 0.50 mM; glassy carbon working electrode, Pt auxiliary electrode, Ag/AgCl/KCl (3 M) reference electrode, 0.1 M KNO_3 supporting electrolyte}.

The redox activity of the Cu(II)—ligand systems in the case of the estradiol derivatives was further studied by the direct redox reaction with GSH and ascorbic acid at pH

7.4 in a 30% (v/v) DMSO/H_2O solvent mixture using UV-vis spectrophotometry. The measurements were conducted using a tandem cuvette under anaerobic conditions. The interaction with both reducing agents resulted in significant spectral changes in the wavelength range of 310–430 nm (Figure 8). As these representative spectra show, the reaction rate with ascorbate was moderate; ca. 1 h was needed to reach the redox equilibrium with 25 equiv. ascorbate. The reduction is accompanied by a decrease in the absorbance band (λ_{max} = 430 nm) belonging to the complex, as the unbound ligand has no absorption in this wavelength range. In the case of GSH, the reaction was so fast that the redox equilibrium was reached immediately after mixing the reactants. The addition of one equiv. of GSH was enough for the complete reduction of the complex, and the resulting Cu(I) ions most probably form complexes with GSH (or its oxidized form), leading to the release of the tridentate ligand. The Cu(II) complexes of both estradiol derivatives displayed similar behavior. The results clearly demonstrate the capability of these Cu(II) complexes to interact with the cellular reducing agent GSH.

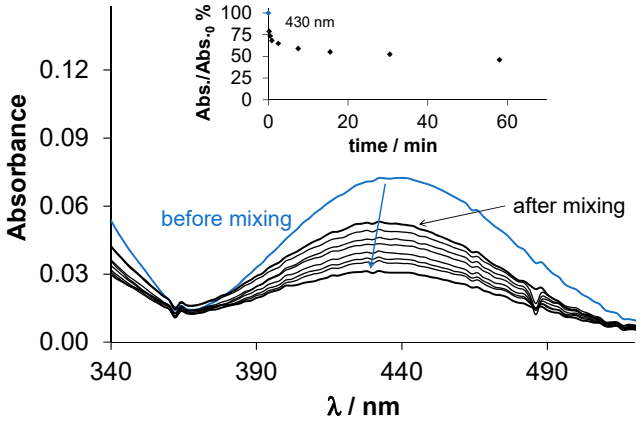

Figure 8. Time-dependent changes of the UV-vis absorption spectra of the Cu(II)—DMA-E2 (1:1) system in the presence of 25 equivalents of ascorbate at pH 7.4 in 30% (v/v) DMSO/H_2O under argon. Inserted figure shows absorbance (Abs.) changes at 430 nm (•) in time. {$c_{Cu(II)} = c_{ligand}$ = 100 μM, $c_{ascorbate}$ = 2.50 mM; pH = 7.4 (20 mM HEPES); T = 25 °C; I = 0.10 M (KCl); ℓ = 1 cm}.

2.5. Synthesis and Characterization of Cu(II) Complexes of PMA-E2 and DMA-E2

As both PMA-E2 and DMA-E2 form stable and redox-active Cu(II) complexes, efforts were made to isolate these complexes from an equimolar solution in a methanol/water mixture. Brown products obtained after washing and drying were characterized by electrospray ionization mass spectrometry (ESI-MS), UV-vis, and EPR spectroscopy. The experimental data for characterization are collected in the Experimental section. The analysis of the data indicated that the general formula of the isolated complexes is [CuLCl] (Chart 3).

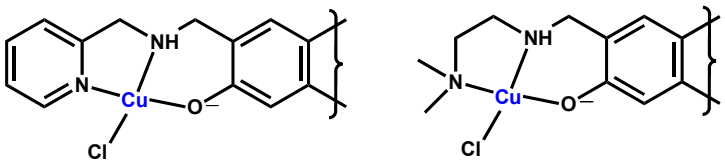

Chart 3. Suggested structures of the isolated [CuLCl] complexes, where HL: PMA-E2 or DMA-E2.

The UV-vis spectra of the complexes in methanol (Figure S13) reveal significant differences from those of the ligands alone, primarily attributed to the emergence of charge-transfer bands in the visible wavelength range. Both the low- and high-resolution ESI-MS spectra (Figures S14–S17) distinctly indicated 1:1 stoichiometry of the metal ion and ligand in the formed complex ([CuL]$^+$), and no free ligands were observed in the samples (except for the DMA-E2 complex, where a higher and higher extent of dissociation was

observed with increasing scan time under the conditions of the high-resolution MS measurement (Figure S17)). The anisotropic g-tensor and A coupling constants obtained from the EPR spectra recorded at 77 K (Figure 9a) are shown in Table S2 together with the EPR parameters of the Cu(II) complexes of DMAP and other ligand-bearing (*N*,*N*,*O*) donor sets. The EPR parameters of the isolated DMA-E2 and PMA-E2 complexes are very similar to those of the $[CuL]^+$ complex of DMAP and the complexes of salicylaldehyde (2-(2-hydroxybenzylidene)hydrazinecarboximidamide (SISC) [36], (E)-2-((3-aminopyridin-2-yl)methylene)hydrazinecarboxamide (oxo-triapine) [37], and the L-phenylalanine derivatives of cis/trans-2-aminocyclohexanecarboxylic acid (c/tACHC) [38]. Based on this similarity, the (*N*,*N*,*O*) coordination mode was proposed for the isolated DMA-E2 and PMA-E2 complexes. However, this tridentate coordination mode can only be confirmed with absolute certainty by X-ray crystallography. PMAP is considered the reduced form of the Schiff base 2-[[(2-pyridinylmethyl)imino]methyl]phenol, and this ligand was found to be coordinated via (N,N,O^-) donor set in its $[CuL]^+$ complex, with the coordination sphere completed by a chorido co-ligand [39]. It should also be noted that no free Cu(II) ions and only mono-ligand complexes were found in the samples based on the EPR spectra. Moreover, the g_0 tensors of the Cu(II) complexes of PMA-E2 and DMA-E2 were compared to those of the complexes formed with other tridentate-sterane-based compounds reported previously [6–8,40] (Figure 9b). The g_0 values of the title complexes are lower than those of the semicarbazones with (*O*,*N*,*O*) donor atoms but are higher than those of thiosemicarbazone complexes bearing (*O*,*N*,*S*) binding sets. Due to the experimental conditions, the co-ligand is a chloride ion, which is most likely replaced by a solvent molecule (H_2O or DMSO) when dissolved in the DMSO/H_2O solvent mixture.

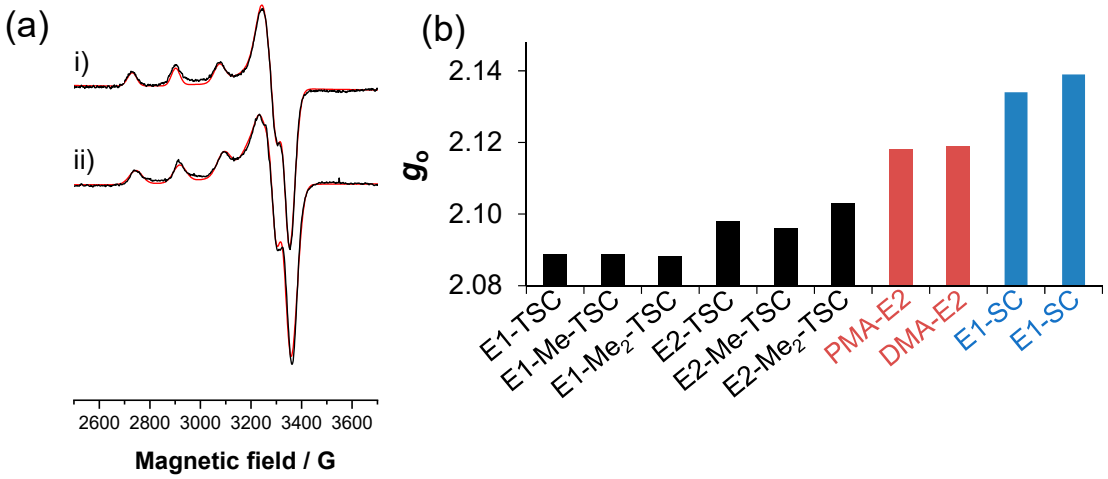

Figure 9. (**a**) Experimental (black) and simulated (red) anisotropic EPR spectra recorded for the [CuLCl] complex of (i) PMA-E2 and (ii) DMA-E2 in DMSO solution. {T = 77 K} The computed anisotropic EPR parameters of the isolated complexes together with reference data of other related complexes [36–38] bearing ligands with (N,N,O^-) donor set are shown in Table S2. (**b**) Calculated g_0 tensors for the [CuLCl] complex of PMA-E2 and DMA-E2 and calculated or experimentally determined g_0 tensors for other sterane-based tridentate ligands for comparison. Color codes for the coordination modes: (*O*,*N*,*S*) donor set: black, (*N*,*N*,*O*) donor set: red; and (*O*,*N*,*O*) donor set: blue. E1-SC and E2-SC are the semicarbazone analogues of E1-TSC and E2-TSC, respectively. Data taken from references [6–8,40].

2.6. In Vitro Cytotoxicity of the Compounds

The cytotoxic activity of PMA-E2, DMA-E2, and their Cu(II) complexes was assayed in MCF-7 human breast and Colo-205 human colon adenocarcinoma cell lines using the colorimetric 3-(4,5-dimethylthiazol-2-yl)-2,5-diphenyl-tetrazolium bromide (MTT) test. Additionally, the cytotoxicity was measured in normal human embryonic lung fibroblast cells (MRC-5). Determined IC_{50} values using a 72 h incubation time are collected in Table 4.

Table 4. In vitro cytotoxicity of PMA-E2, DMA-E2, and their Cu(II) complexes expressed as IC_{50} values in MCF-7 breast cancer, Colo-205 human colon adenocarcinoma, and MRC-5 human lung fibroblast cells. IC_{50} values are also shown for the positive control doxorubicin and for other sterane-based hybrids (Chart 1) determined under identical conditions. {Exposition time: 72 h}.

IC_{50}/μM	MCF-7	Colo-205	MRC-5
PMA-E2	62.56 ± 0.62	42.4 ± 1.1	34.7 ± 1.7
DMA-E2	60.2 ± 1.1	29.9 ± 1.0	14.95 ± 0.22
[Cu(PMA-E2H$_{-1}$)Cl]	31.89 ± 0.61	15.25 ± 0.48	24.46 ± 0.31
[Cu(DMA-E2H$_{-1}$)Cl]	45.36 ± 0.31	18.27 ± 0.28	13.85 ± 0.55
$CuCl_2$	54.4 ± 1.8	32.79 ± 0.83	39.9 ± 1.3
E1-TSC [a]	6.42 ± 0.40	20.3 ± 1.4	22.6 ± 3.5
[Cu(E1–TSCH$_{-2}$)] [a]	0.57 ± 0.03	1.99 ± 0.19	1.59 ± 0.13
E2-salicylhydroxamic acid [b]	25.2 ± 0.8	58.6 ± 1.4	>100
2-amino-E2 [c]	>100	17.3 ± 0.1	>100
doxorubicin [b]	0.21 ± 0.03	0.64 ± 0.06	1.16 ± 0.15

[a] Data are taken from Ref. [6]. [b] Data are taken from Ref. [9]. [c] Data are taken from Ref. [10].

In light of the IC_{50} values, both sterane-based ligands exhibit a moderate level of cytotoxicity in all cells tested. There are no significant differences between the IC_{50} values of the ligands, and regrettably, they do not display selectivity for cancer cells over normal cells. Meanwhile, in our previous work, the conjugation with a different metal chelating moiety to the estradiol scaffold resulted in a compound, E2-salicylhydroxamic acid (Chart 1), with similar or somewhat better cytotoxic activity than these E2 derivatives (Table 4), but with increased selectivity [9]. Comparing the activity of PMA-E2 and DMA-E2 to that of 2-amino-E2 [10] (Table 4), it can be concluded that they were more cytotoxic in breast cancer cells while displaying weaker activity in Colo-205 cells. Notably, both PMA-E2 and DMA-E2 were less cytotoxic when compared to the tridentate thiosemicarbazone-estrone derivative [8] (Table 4).

The Cu(II) complexes formed with PMA-E2 and DMA-E2 displayed notably enhanced anticancer activity when compared to the non-coordinated ligand, and their selectivity towards the cancer cells is slightly stronger than that of the corresponding ligands. Furthermore, these complexes showed greater cytotoxicity than the $CuCl_2$ salt itself. It is also noteworthy that the cytotoxic activity of the reference compound PMAP and its Cu(II) complex was characterized by higher IC_{50} values in various cancer cells [27], including Colo-205, than the corresponding PMA-E2 and its complex.

3. Materials and Methods

3.1. Chemicals

KCl, HCl, KOH, DMSO, DMSO-d_6, D_2O, $CDCl_3$, DMF, tetrabutylammonium nitrate (TBAN), 4-(2-hydroxyethyl)-1-piperazineethanesulfonic acid (HEPES), and 4,4-dimethyl-4-silapentane-1-sulfonic acid (DSS) were obtained from Sigma-Aldrich (St Louis, MO, USA) in puriss quality. For the Cu(II) stock solution, $CuCl_2$ was dissolved in water, and the concentration was determined by complexometric titrations with EDTA. Milli-Q water was used for sample preparation.

Chemicals, reagents, and solvents were purchased from commercial suppliers (Sigma-Aldrich, and Alfa Aesar, Haverhill, MA, USA) and used for the synthesis of the ligands and the complexes without further purification. The transformations were monitored by TLC using 0.25 mm-thick Kieselgel-G plates (Si 254 F, Merck, New York, NY, USA). Compound spots were detected by spraying with 5% phosphomolybdic acid in 50% aqueous phosphoric acid or with 1% *p*-anisaldehyde in a mixture of 50 mL glacial acetic acid and 1 mL of *cc* sulfuric acid. Flash chromatographic purifications were carried out on silica gel 60, 40–63 μm (Merck). All eluent compositions are given in volume percent (% (*v*/*v*)).

3.2. General Procedure for the Synthesis of Secondary Amines (PMAP, DMAP, PMA-E2, and DMA-E2) via Reductive Amination

Salicylaldehyde (214 µL, 2.0 mmol) or 2-formylestrone (F-E1, 597 mg, 2.0 mmol, prepared via Casiraghi formylation [30]) was dissolved in MeOH (5 mL), then anhydrous Na_2SO_4 (100 mg) and the corresponding amine (2.0 mmol, 1 equiv.) were added, and the reaction mixture was kept at reflux temperature for 3 h. The solution was then cooled to 0 °C, $NaBH_4$ (76 mg, 2.0 mmol) was added in small portions, and the stirring was continued for another 1 h. The mixture was poured onto water, quenched with 10% (*m*/*m*) HCl, its pH was adjusted to 10 with a 2 M NaOH solution, and it was then extracted with ethyl acetate (EtOAc) (3 × 10 mL). The combined organic layers were washed with water and brine, dried over anhydrous $MgSO_4$, and evaporated in vacuo. The crude product was purified by column chromatography.

For the characterization of the ligands, the NMR spectra were recorded with a Bruker Ultrashield 500 Plus Instrument (Billerica, MA, USA) at room temperature in $CDCl_3$ or DMSO-d_6 using residual solvent signals as an internal reference (Figures S1–S8). Chemical shifts are reported in ppm (δ scale), and coupling constants (J) are given in Hz. Multiplicities of the ^{1}H signals are indicated as a singlet (s), a doublet (d), a doublet of doublets (dd), a triplet (t), a triplet of doublets (td), a doublet of triplets (dt), or a multiplet (m). ^{13}C NMR spectra are ^{1}H-decoupled, and the J-MOD pulse sequence was used for multiplicity editing. In this spin-echo-type experiment, the signal intensity is modulated by the different coupling constants J of carbons depending on the number of attached protons. Both protonated and unprotonated carbons can be detected (CH_3 and CH carbons appear as positive signals, while CH_2 and C carbons are negative signals).

3.2.1. 2-((((Pyridin-2-yl)methyl)amino)methyl)phenol (PMAP)

According to the general procedure, salicylaldehyde and 2-picolylamine (206 µL) were used. The crude product was purified with MeOH/dichloromethane (DCM) = 0:100 to 10:90 (gradient). Yield: 157 mg (37%, brown oil). ^{1}H NMR (500 MHz, $CDCl_3$): δ_H 3.93 (s, 2H, CH_2), 4.01 (s, 2H, CH_2), 6.78 (td, *J* = 7.4, 1.2 Hz, 1H), 6.86 (dd, *J* = 8.1, 1.2 Hz, 1H), 6.93–7.00 (m, 1H), 7.14–7.24 (m, 3H), 7.66 (td, *J* = 7.7, 1.8 Hz, 1H), 8.54–8.61 (m, 1H); ^{13}C NMR (125 MHz, $CDCl_3$): δ_C 52.0 (CH_2), 53.2 (CH_2), 116.6, 119.2, 122.5 (C), 122.6 (CH), 122.8 (CH), 128.8 (CH), 129.0 (CH), 129.1 (CH), 136.8 (CH), 149.6 (CH), 157.9 (C), 158.4 (C).

3.2.2. 2-(((2-(Dimethylamino)ethyl)amino)methyl)phenol (DMAP)

According to the general procedure, salicylaldehyde and *N*,*N*-dimethylethylenediamine (218 µL) were used. The crude product was purified with MeOH/DCM = 0:100 to 10:90 (gradient). Yield: 119 mg (31%, brown oil). ^{1}H NMR (500 MHz, D_2O): δ_H 2.92 (s, 3H, one of the N-Me), 2.93 (s, 3H, the other N-Me), 3.44–3.55 (m, 4H, 2 × CH_2), 4.30 (s, 2H, benzylic CH_2), 6.99–7.06 (m, 2H), 7.35–7.43 (m, 2H); ^{13}C NMR (125 MHz, D_2O): δ_C 41.3 (CH_2), 43.3 (2 × N-CH_3), 47.5 (CH_2), 53.0 (CH_2), 115.7 (CH), 117.6 (C), 120.7 (CH), 131.6 (CH), 131.7 (CH), 155.1 (C).

3.2.3. 2-((((2-Pyridin-2-yl)methyl)amino)methyl)estradiol (PMA-E2)

According to the general procedure, F-E1 and 2-picolylamine (206 µL) were used. The crude product was purified with MeOH/DCM = 0:100 to 10:90 (gradient). Yield: 605 mg (77%, yellow-brown oil). ^{1}H NMR (500 MHz, $CDCl_3$): δ_H 0.78 (s, 3H, 18-H_3), 1.13–1.53 (overlapping m, 7H), 1.65–1.75 (m, 1H), 1.82–1.90 (m, 1H), 1.93 (dt, *J* = 12.6, 3.3 Hz, 1H), 2.06–2.19 (m, 2H), 2.22–2.37 (m, 1H), 2.77–2.88 (m, 2H, 6-H_2), 3.72 (t, *J* = 8.5 Hz, 1H), 3.93–4.04 (overlapping m, 4H, benzylic and aminomethyl CH_2), 6.60 (s, 1H, 4-H), 6.90 (s, 1H, 1-H), 7.20–7.25 (overlapping m, 2H), 7.67 (td, *J* = 7.6, 1.8 Hz, 1H), 8.58 (dt, *J* = 4.8, 1.3 Hz, 1H); ^{13}C NMR (125 MHz, $CDCl_3$): δ_C 11.2 (C-18), 23.3 (CH_2), 26.6 (CH_2), 27.4 (CH_2), 29.5 (CH_2), 30.8 (CH_2), 36.9 (CH_2), 39.1 (CH), 43.4 (C-13), 44.1 (CH), 50.2 (CH), 52.0 (N-CH_2), 53.1 (N-CH_2), 82.1 (C-17), 116.5 (C-4), 119.7 (C-2), 122.6 (CH), 122.9 (CH), 125.8 (C-1), 131.2 (C-10), 136.9 (CH), 137.6 (C-5), 149.5 (CH), 155.8 (C-3), 157.8 (pyridine C).

3.2.4. 2-(((2-(Dimethylamino)ethyl)amino)methyl)estradiol (DMA-E2)

According to the general procedure, F-E1 and *N*,*N*-dimethylethylenediamine (218 µL) were used. The crude product was purified with EtOAc/triethylamine = 95:5. Yield: 358 mg (48% yellow, viscous oil). ^{1}H NMR (500 MHz, $CDCl_3$): δ_H 0.77 (s, 3H, 18-H_3), 1.13–1.53 (m, 7H), 1.64–1.74 (m, 1H), 1.81–1.89 (m, 1H), 1.93 (dt, *J* = 12.6, 3.3 Hz, 1H), 2.05–2.19 (m, 2H), 2.22 (s, 6H, 2 × N-CH_3), 2.24–2.32 (m, 1H), 2.44 (dd, *J* = 6.6, 5.1 Hz, 2H, one of N-CH_2), 2.72 (dd, *J* = 6.5, 5.1 Hz, 2H, the other N-CH_2), 2.74–2.87 (m, 2H, 6-H_2), 3.72 (t, *J* = 8.5 Hz, 1H, 17-H), 3.90–4.00 (m, 2H, aminomethyl CH_2), 6.56 (s, 1H, 4-H), 6.90 (s, 1H, 1-H); ^{13}C NMR (125 MHz, $CDCl_3$): δ_C 11.2 (C-18), 23.3 (CH_2), 26.6 (CH_2), 27.5 (CH_2), 29.5 (CH_2), 30.8 (CH_2), 36.9 (CH_2), 39.1 (CH), 43.4 (C-13), 44.0 (CH), 45.5 (2 × N-CH_3), 45.8 (N-CH_2), 50.2 (CH), 52.6 (N-CH_2), 58.3 (N-CH_2), 82.1 (C-17), 116.4 (C-4), 120.1 (C-2), 125.4 (C-1), 130.9 (C-10), 137.3 (C-5), 156.0 (C-3).

3.3. Synthesis and Characterization Cu(II) Complexes of PMA-E2 and DMA-E2

A solution containing the ligands PMA-E2 or DMA-E2 (0.05 mmol) was prepared by dissolving them in 20 mL of MeOH. Subsequently, a 0.40 mL aqueous solution of $CuCl_2$ (0.05 mmol) was introduced. The solution was stirred for a duration of 5 h at a temperature of 60 °C. Afterward, it was allowed to cool, and the pH was carefully adjusted to approximately 7.4 by adding 10 mM HEPES (5 mL). In the case of both ligands, a brown precipitate formed, which was decanted, followed by a washing step with water (10 mL) and subsequent drying overnight at 50 °C. The Cu(II) complexes were characterized using ESI-MS, UV-vis, and EPR spectroscopy (Figure 9 and Figures S13–S15).

Complex of PMA-E2 as [CuLCl]: yield: 88%; low-resolution ESI-MS (methanol, positive): m/z $[CuL]^+$ found 454.17, calcd. 454.19 (Figure S14), and high-resolution ESI-MS (methanol, positive): m/z $[CuL]^+$ found 454.1679, calcd. 454.1682 (Figure S15) for $C_{25}H_{31}N_2O_2Cu$; λ_{max} (nm) in methanol: 292 and 434 nm. EPR parameters (77 K): $g_\perp$ = 2.051, $g_\parallel$ = 2.256, $A_\perp = 20\times10^{-4}$ cm^{-1}, $A_\parallel = 178 \times 10^{-4}$ cm^{-1}, $g_{0,calcd}$ = 2.119.

Complex of DMA-E2 as [CuLCl]: yield: 82%; low-resolution ESI-MS (methanol, positive): m/z $[CuL]^+$ found 434.22, calcd. 434.20 (Figure S16), and high-resolution ESI-MS (methanol, positive): m/z $[CuL]^+$ found 434.1992, calcd. 434.1995 (Figure S17) for $C_{23}H_{35}N_2O_2Cu$; λ_{max} (nm) in methanol: 282, 381 and 465 nm. EPR parameters (77 K): $g_\perp$ = 2.055, $g_\parallel$ = 2.244, $A_\perp = 27 \times 10^{-4}$ cm^{-1}, $A_\parallel = 177 \times 10^{-4}$ cm^{-1}, $g_{0,calcd}$ = 2.118.

Low-resolution ESI-MS measurements were performed using a Brucker Amazon Speed with ETD (Billerica, MA, USA) ion trap mass spectrometer. Spectra (Figures S14 and S15) were recorded by direct infusion with a sample concentration of ~5 µM and a flow rate of 0.24 mL/h. The eluent was an acetonitrile/methanol = 1:1 mixture with 1% H_2O. Samples were measured with the following settings: dry temperature 180 °C, nebulizer 8.00 psi, dry gas 6 L/min, and the high voltage capillary was set to 4.5 kV for positive mode, and the m/z 200–1000 mass region was monitored. The high-resolution mass spectra (Figures S16–S18) were acquired in the range of 100 to 1100 m/z with a Q Exactive Plus quadrupole-orbitrap mass spectrometer (Thermo Fisher Scientific, Waltham, MA, USA) equipped with a heated electrospray (HESI). Analyses were performed in positive ion mode using flow injection mass spectrometry with a mobile phase of 100% methanol. The flow rate was 0.3 mL/min. 5 µL aliquots of the samples were loaded into the flow. The ESI capillary was adjusted to 3.5 kV, and nitrogen was used as a nebulizer gas. For the characterization, an Agilent Cary 8454 spectrophotometer (Agilent Technologies, Santa Clara, CA, USA) was applied to record the UV-vis spectrum of the prepared complexes and the ligands in MeOH. For measurements of the anisotropic EPR spectra, see Section 3.7.

3.4. pH-Potentiometry

pH-Potentiometric titrations were performed at a temperature of 25.0 ± 0.1 °C in solutions consisting of 30% (*v*/*v*) DMSO/H_2O with an ionic strength of 0.10 M (KCl) for the determination of the proton dissociation constants of the ligands as well as the overall stability constants of the Cu(II) complexes of PMAP and DMAP. The titrations were

conducted using a carbonate-free KOH solution with a known concentration of 0.10 M. The exact concentrations of the base and the HCl were determined by pH-potentiometric titrations. An Orion 710A pH-meter equipped with a Metrohm combined electrode (type 6.0234.100) and a Metrohm 665 Dosimat burette were applied for the titrations. The electrode system was calibrated to the pH = $-\log[H^+]$ scale by blank titrations (strong acid vs. strong base: HCl vs. KOH) according to the method suggested by Irving et al. [41]. The average water ionization constant pK_w was 14.52 ± 0.05. The pH-potentiometric titrations were conducted in the pH range of 2.0–12.5. The initial volume of the samples was 10.0 mL. The ligand concentration was 2 or 3 mM for the model compounds (PMAP, DMAP), and metal ion-to-ligand ratios of 1:1–1:2 were used. For the estadiol derivatives (PMA-E2, DMA-E2), more diluted solutions (0.5 mM) were used. Argon was always passed over the solutions during the titrations. The exact concentration of the ligand stock solutions and the proton dissociation constants were determined by pH-potentiometric titrations with the use of the computer program HYPERQUAD [42]. This program was also used to establish the stoichiometry of the complexes and to compute the stability constants ($\beta(M_pL_qH_r)$). $\beta(M_pL_qH_r)$ is defined for the general equilibrium $pM + qL + rH \rightleftharpoons M_pL_qH_r$ as $\beta(M_pL_qH_r) = [M_pL_qH_r]/[M]^p[L]^q[H]^r$, where M denotes the metal ion and L the completely deprotonated ligand. In all calculations exclusively, titration data were used from experiments in which no precipitate was visible in the reaction mixture.

3.5. UV-Vis Spectrophotometry

For most of the UV-vis spectra, an Agilent Cary 3500 spectrophotometer (Agilent Technologies, Santa Clara, CA, USA) was used at an interval of 200–800 nm. The path length was 1 cm.

Titrations: Spectrophotometric titrations were performed in 30% (*v*/*v*) DMSO/H_2O on samples containing the ligands at 50 μM (PMA-E2, DMA-E2) or 300 μM (PMAP, DMAP) concentrations in the pH range from 1.0 to 12.5 in the absence or in the presence of 1.0, 0.67, or 0.5 equiv. Cu(II) ions. pK_a values of the ligands, logβ values of the metal complexes, and the UV-vis spectra of the individual species were calculated by the computer program PSEQUAD [43].

Redox reaction with GSH: The redox reaction involving the Cu(II) complexes of PMA-E2 and DMA-E2 with GSH and ascorbic acid was investigated in 30% (*v*/*v*) DMSO/H_2O at 25.0 ± 0.1 °C using a special, tightly closed tandem cuvette (Hellma Tandem Cell, 238-QS). The reactants were separated until the reaction was triggered. The cuvette's isolated pockets were thoroughly deoxygenated by purging with a stream of argon for 10 min prior to the mixture of reactants. Spectra were recorded using an Agilent Cary 8454 diode array spectrophotometer (Agilent Technologies, Santa Clara, CA, USA) both before and immediately after the mixing procedure. The monitoring of spectral changes persisted until no further alterations in absorbance were detected. One of the isolated pockets contained the metal complex, while the other contained a reducing agent (1–50 equiv.). The final concentration of the complex after mixing was 100 or 150 μM. The pH of all the solutions was adjusted to 7.40 by 50 mM HEPES buffer, and an ionic strength of 0.1 M (KCl) was applied. Fresh stock solutions of both the reducing agents and the complexes were prepared on a daily basis.

Solubility: Thermodynamic solubility ($S_{7.4}$) of PMA-E2 and DMA-E2 was assessed by measuring the saturation levels in water at pH 7.40 (10 mM HEPES buffer) at 25.0 ± 0.1 °C. The concentration of the compounds was determined by UV-vis spectrophotometry. For calibration, stock solutions of the compounds were used with known concentrations dissolved in 100% DMSO and 50% (*v*/*v*) DMSO/buffered aqueous solutions.

Lipophilicity: Distribution coefficients ($D_{7.4}$) of PMA-E2 and DMA-E2 were determined by the traditional shake-flask method in an *n*-octanol/buffered aqueous solution at pH 7.40 (20 mM HEPES, 0.10 M KCl) at 25.0 ± 0.2 °C, as described previously [44].

3.6. ^{1}H NMR Spectroscopic Titrations

^{1}H NMR titrations for the ligands PMAP and DMAP (c ~300 μM) were carried out on a Bruker Ultrashield 500 Plus instrument (Billerica, MA, USA). DSS was used as an internal NMR standard, and the WATERGATE water suppression pulse scheme was used. Spectra were recorded in 10% (*v*/*v*) D_2O/H_2O or in 30% (*v*/*v*) DMSO-d_6/H_2O solvent mixtures at a concentration of 1 mM, respectively, at an ionic strength of 0.10 M (KCl).

3.7. EPR Spectroscopic Measurements and Evaluation of the Spectra

CW X-band EPR spectra were recorded with a BRUKER EleXsys E500 spectrometer. Microwave power of 13 mW, modulation amplitude of 5 G, and modulation frequency of 100 kHz were used. Titrations have been performed for Cu(II)—DMAP and Cu(II)—DMA-E2 at 2.84 mM Cu(II) and 3.0 mM ligand and 0.43 mM Cu(II) and 0.55 mM ligand concentrations, respectively, in a 30% (*v*/*v*) DMSO/H_2O solution mixture. The titrations were performed with KOH solution (with 30% DMSO), and the ionic strength was set to 0.1 M (KCl). Room temperature measurements were performed in capillaries at different pH values between pH 2–12 using 4 scans. During the titrations, samples of 0.2 mL were transferred into quartz EPR tubes and measured in a dewar containing liquid nitrogen (77 K) to obtain the pH-dependent frozen solution EPR spectra. The spectrum of the 30% (*v*/*v*) DMSO/water solvent mixture as a background was subtracted from the measured spectra to correct the baseline.

The series of pH-dependent isotropic EPR spectra were simulated simultaneously by the '2d_epr' software [45]. To describe the component spectra, the isotropic parameters g_0, A_0^{Cu} copper hyperfine ($I_{Cu} = 3/2$), and two equivalent a_0^N nitrogen ($I_N = 1$) superhyperfine couplings have been taken into account. The relaxation parameters α, β, and γ defined the linewidths through the equation $\sigma_{MI} = \alpha + \beta M_I + \gamma M_I^2$, where M_I denotes the magnetic quantum number of the paramagnetic metal ions. The concentration of the components was calculated with the help of the formation constants of the complexes (logβ values) determined by pH-potentiometry.

Anisotropic EPR spectra were simulated one-by-one by the EPR software [46]. Axial g- and copper hyperfine A^{Cu}-tensors were taken into account. Two equivalents, isotropic nitrogen couplings (a_0^N), were taken into account in the spectrum simulations. For the description of the linewidth, the orientation-dependent relaxation parameters (α, β, and γ) were used. Since a natural $CuCl_2$ was used for the measurements, spectra were calculated as the sum of the spectra of ^{63}Cu and ^{65}Cu weighted by their natural abundances.

Anisotropic EPR spectra were also recorded for the isolated Cu(II) complexes of PMA-E2 and DMA-E2. Powder of the Cu(II) complexes was dissolved in DMSO to obtain approximately 3 mM concentration solutions. 0.20 mL samples were transferred into quartz EPR tubes, and the spectra were recorded in a dewar containing liquid nitrogen (77 K).

3.8. Cyclic Voltammetry

Cyclic voltammograms for the Cu(II)—DMAP, DMA-E2, and PMAP systems were recorded at 25.0 ± 0.1 °C in 30% (*v*/*v*) DMF/H_2O at pH 7.4. The samples contained 0.50 mM $Cu(NO_3)_2$ and 0.55 or 0.60 mM ligand. Ionic strength was 0.10 M (KNO_3). Measurements were performed on a conventional three-electrode system under a nitrogen atmosphere using an Autolab PGSTAT 204 potentiostat/galvanostat monitored by Metrohm's Nova software. Samples were purged with argon for 15 min before recording the cyclic voltammograms. Glassy carbon and platinum electrodes were used as working and auxiliary electrodes, respectively, and Ag/AgCl/3 M KCl served as a reference electrode. The electrochemical system was calibrated with an aqueous solution of $K_3[Fe(CN)_6]$ ($E_{1/2}$ = +0.458 V vs. NHE).

3.9. In Vitro Cell Studies: Cell Lines and Culture Conditions and MTT Assay

All cell culture reagents were obtained from Sigma-Aldrich and plasticware from Sarstedt (Nümbrecht, Germany). The human MCF-7 breast cancer cell line and the human

colon Colo-205 (CCL-222, ATCC, Manassas, VA, USA) adenocarcinoma cell line were purchased from LGC Promochem, Teddington, UK. The MRC-5 human embryonal lung fibroblast cell line (CCL-171, ATCC) is from Sigma-Aldrich (Merck KGaA, Darmstadt, Germany). The Colo-205 cancer cells were cultured in Roswell Park Memorial Institute (RPMI) 1640 medium supplemented with 10% heat-inactivated fetal bovine serum, 2 mM L-glutamine, 1 mM sodium pyruvate, and 10 mM HEPES. The MCF-7 and MRC-5 cell lines were cultured in Eagle's Minimal Essential Medium (EMEM, Sigma-Aldrich, St. Louis, MO, USA) containing 4.5 g/L of glucose and supplemented with a non-essential amino acid mixture, a selection of vitamins, and 10% FBS. The cells were incubated at 37 °C in a 5% CO_2 and 95% air atmosphere. All cell lines were detached with Trypsin-Versene (EDTA) solution for 5 min at 37 °C.

The tested compounds (PMA-E2, DMA-E2, and their Cu(II) complexes) were dissolved in 90% (*v*/*v*) DMSO/H_2O using a 5 mM concentration, and in the final samples, the DMSO content was always lower than 1%. Then, stock solutions were diluted in complete culture medium, and two-fold serial dilutions of compounds were prepared in 100 µL of the medium, horizontally. The cells were treated with a Trypsin-Versene (EDTA) solution. They were adjusted to a density of 1×10^4 cells in 100 µL of RPMI 1640 or EMEM medium and were added to each well, with the exception of the medium control wells. The MCF-7 and MRC-5 cells were seeded for 4 h prior to the assay. The final volume of the wells containing compounds and cells was 200 µL. The plates containing MCF-7, Colo-205, or MRC-5 cells were incubated at 37 °C for 72 h; at the end of the incubation period, 20 µL of MTT solution (from a stock solution of 5 mg/mL) were added to each well. After incubation at 37 °C for 4 h, 100 µL of SDS solution (10% in 0.01 M HCI) were added to each well, and the plates were further incubated at 37 °C overnight.

Cell growth was determined by measuring the optical density (OD) at 540/630 nm with a Multiskan EX plate reader (Thermo Labsystems, Cheshire, WA, USA). Inhibition of cell growth (expressed as IC_{50}: inhibitory concentration that reduces by 50% the growth of the cells exposed to the tested compounds) was determined from the sigmoid curve, where $100 - ((OD_{sample} - OD_{medium\ control})/(OD_{cell\ control} - OD_{medium\ control})) \times 100$ values were plotted against the logarithm of compound concentrations. Curves were fitted by GraphPad Prism software (2021, GraphPad Software, San Diego, CA, USA) [47] using the sigmoidal dose–response model (comparing variable and fixed slopes). The IC_{50} values were obtained from at least 3 independent experiments.

4. Conclusions

Two estradiol-based hybrids bearing (*N*,*N*,*O*) donor sets were developed and studied for their solubility, lipophilicity, proton dissociation, and complex formation equilibrium processes with Cu(II) ions, in addition to their cytotoxic activity. The deprotonation processes were followed by UV-vis, pH-potentiometric, and ^{1}H NMR titrations, and to validate the obtained proton dissociation constants, two structurally analogous compounds, PMAP and DMAP, with much better aqueous solubility, were included. All ligands have three dissociable protons in their fully protonated forms in the studied pH range. It was found that the sterane conjugation has a significant effect on the pK_a values attributed to the phenolic hydroxyl group on the A-ring; namely, the deprotonation of this moiety occurs at higher pH values in the case of the estradiol derivatives due to the electron-donating effect of the sterane scaffold. On the basis of the determined pK_a values, the H_2L^+ form predominates for DMA-E2 and DMAP at pH 7.4, while the other two compounds are found partly in their neutral forms (PMA-E2: 66% H_2L^+, 34% HL; and PMAP: 63% H_2L^+, 37% HL).

The solution speciation model for the Cu(II) complexes was found to be rather simple in all cases under the conditions applied, namely, the formation of only mono-ligand complexes $[CuL]^+$ and $[CuLH_{-1}]$. It was concluded that complex $[CuL]^+$ is the sole species at pH 7.4 with all the studied ligands, in which the ligand is coordinated via the (N,N,O^-) donor set. The spectral changes in the UV-vis spectra suggest that the complex

[$CuLH_{-1}$] is formed by the metal-induced deprotonation of the secondary nitrogen. To confirm the proposed speciation model and to elucidate the coordination mode in each complex, EPR spectroscopic measurements were performed for DMA-E2 and its model. Deconvolution of the EPR spectra showed that only two types of complexes are formed in the solution even at ligand excess, which were also identified as $[CuL]^+$ and [$CuLH_{-1}$]. The corresponding complexes of DMA-E2 and DMAP have similar g_0 tensor and A_0 coupling constants; however, the relaxation parameters are different, and the rotational averaging of the direction-dependent parameter appears to be incomplete compared to the complexes of the less rigid model ligand. From the formation constants, it could be concluded that all four ligands form highly stable Cu(II) complexes, and their dissociation is negligible at pH 7.4 at a concentration of 10 μM. The stability of the Cu(II) complexes with the pyridine nitrogen-containing PMA-E2 and PMAP is somewhat higher than that of the compounds bearing the tertiary ammonium group. The Cu(II) complexes were characterized by relatively low redox potentials, indicating a weaker oxidizing power, although they could be reduced by ascorbate and GSH.

The Cu(II) complexes of PMA-E2 and DMA-E2 were isolated in [CuLCl] forms and tested for their cytotoxicity in human breast (MCF-7) and colon adenocarcinoma (Colo-205) cells, as well as in a non-cancerous human embryonal lung fibroblast cell line (MRC-5). The sterane hybrids exhibited moderate cytotoxic activity without selectivity, while their Cu(II) complexes were more cytotoxic with a slightly better selectivity profile.

Supplementary Materials: The following supporting information can be downloaded at: https://www.mdpi.com/article/10.3390/inorganics12020049/s1; Figures S1–S8: ^1H and ^{13}C NMR spectra of PMAP, DMAP, PMA-E2, and DMA-E2; Figure S9: Time-dependent ^1H NMR spectra of the ligands; Figures S10 and S11: EPR spectra of the Cu(II)—DMAP/DMA-E2 systems; Figure S12: Concentration distribution curves for the Cu(II)—DMAP/DMA-E2 systems; Figure S13: UV-vis spectra of PMA-E2 and DMA-E2 and their Cu(II) complexes in MeOH; Figures S14–S18: ESI-MS spectra of the Cu(II) complexes of PMA-E2 and DMA-E2; Table S1: Electrochemical data for the Cu(II)—DMAP/DMA-E2/PMAP systems; Table S2: Anisotropic EPR parameters of complexes for comparison. References [36–38] are cited in the supplementary materials.

Author Contributions: Conceptualization, É.A.E.; investigation, A.G., T.V.P., F.K. and B.M.; formal analysis, J.P.M., N.V.M., G.S. and É.A.E.; writing—original draft preparation, É.A.E.; writing—review and editing, É.A.E., É.F., N.V.M. and G.S.; funding acquisition, É.A.E. All authors have read and agreed to the published version of the manuscript.

Funding: This research was funded by the National Research, Development, and Innovation Office (NKFIA) through project TKP-2021-EGA-32, the "Lendület" Programme (HUN-REN Hungarian Research Network, LP2019-6/2019), and the ÚNKP-22-5-SZTE-588 New National Excellence program of the Ministry for Innovation and Technology.

Data Availability Statement: The data used to support the findings of this work are available from the corresponding author upon request.

Conflicts of Interest: The authors declare no conflicts of interest.

References

1. Bansal, R.; Acharya, P.C. Man-made cytotoxic steroids: Exemplary agents for cancer therapy. *Chem. Rev.* **2014**, *114*, 6986–7005. [CrossRef]
2. Minorics, R.; Zupkó, I. Steroidal anticancer agents: An overview of estradiol-related compounds. *Anticancer Agents Med. Chem.* **2018**, *18*, 652–666. [CrossRef]
3. Marchesi, E.; Perrone, D.; Navacchia, M.L. Molecular hybridization as a strategy for developing artemisinin-derived anticancer candidates. *Pharmaceutics* **2023**, *15*, 218. [CrossRef]
4. Bansal, R.; Surya, A. A comprehensive review on steroidal bioconjugates as promising leads in drug discovery. *ACS Bio Med Chem Au* **2022**, *2*, 340–369. [CrossRef] [PubMed]
5. Zolottsev, V.A.; Latysheva, A.S.; Pokrovsky, V.S.; Khan, I.I.; Misharin, A.Y. Promising applications of steroid conjugates for cancer research and treatment. *Eur. J. Med. Chem.* **2021**, *210*, 113089. [CrossRef]

6. Petrasheuskaya, T.V.; Kiss, M.A.; Dömötör, O.; Holczbauer, T.; May, N.V.; Spengler, G.; Kincses, A.; Gašparović, A.Č.; Frank, É.; Enyedy, É.A. Salicylaldehyde thiosemicarbazone copper complexes: Impact of hybridization with estrone on cytotoxicity, solution stability and redox activity. *New J. Chem.* **2020**, *44*, 12154–12168. [CrossRef]
7. Petrasheuskaya, T.V.; Wernitznig, D.; Kiss, M.A.; May, N.V.; Wenisch, D.; Keppler, B.K.; Frank, É.; Enyedy, É.A. Estrone–salicylaldehyde N-methylated thiosemicarbazone hybrids and their copper complexes: Solution structure, stability and anticancer activity in tumour spheroids. *J. Biol. Inorg. Chem.* **2021**, *26*, 775–791. [CrossRef] [PubMed]
8. Petrasheuskaya, T.V.; Kovács, F.; Igaz, N.; Rónavári, A.; Hajdu, B.; Bereczki, L.; May, N.V.; Spengler, G.; Gyurcsik, B.; Kiricsi, M.; et al. Estradiol-based salicylaldehyde (thio)semicarbazones and their copper complexes with anticancer, antibacterial and antioxidant activities. *Molecules* **2023**, *28*, 54. [CrossRef] [PubMed]
9. Mészáros, J.P.; Kovács, H.; Spengler, G.; Kovács, F.; Frank, É.; Enyedy, É.A. A comparative study on the metal complexes of an anticancer estradiol-hydroxamate conjugate and salicylhydroxamic acid. *J. Inorg. Biochem.* **2023**, *244*, 112223. [CrossRef] [PubMed]
10. Petrasheuskaya, T.V.; Kovács, F.; Spengler, G.; May, N.V.; Frank, É.; Enyedy, É.A. A comparative study on the complex formation of 2-aminoestradiol and 2-aminophenol with divalent metal ions: Solution chemistry and anticancer activity. *J. Mol. Struct.* **2022**, *1261*, 132858. [CrossRef]
11. Molnár, B.; Kinyua, N.I.; Mótyán, G.; Leits, P.; Zupkó, I.; Minorics, R.; Balogh, G.T.; Frank, É. Regioselective synthesis, physicochemical properties and anticancer activity of 2-aminomethylated estrone derivatives. *J. Steroid Biochem. Mol. Biol.* **2022**, *219*, 106064. [CrossRef] [PubMed]
12. Biersack, B.; Schobert, R. Metallodrug conjugates with steroids and selective estrogen receptor modulators (SERM). *Curr. Med. Chem.* **2009**, *16*, 2324–2337. [CrossRef] [PubMed]
13. Le Bideau, F.; Dagorne, S. Synthesis of transition-metal steroid derivatives. *Chem. Rev.* **2013**, *113*, 7793–7850. [CrossRef] [PubMed]
14. Gust, R.; Beck, W.; Jaouen, G.; Schönenberger, H. Optimization of cisplatin for the treatment of hormone dependent tumoral diseases: Part 1: Use of steroidal ligands. *Coord. Chem. Rev.* **2009**, *253*, 2742–2759. [CrossRef]
15. Altman, J.; Castrillo, T.; Beck, W.; Bernhardt, G.; Schoenenberger, H. Metal complexes with biologically important ligands. 62. Platinum (II) complexes of 3-(2-aminoethoxy) estrone and-estradiol. *Inorg. Chem.* **1991**, *30*, 4085–4088. [CrossRef]
16. Kitteringham, E.; Andriollo, E.; Gandin, V.; Montagner, D.; Griffith, D.M. Synthesis, characterisation and in vitro antitumour potential of novel Pt (II) estrogen linked complexes. *Inorg. Chim. Acta* **2019**, *495*, 118944. [CrossRef]
17. Seroka, B.; Łotowski, Z.; Wojtkielewicz, A.; Bazydło, P.; Dudź, E.; Hryniewicka, A.; Morzycki, J.W. Synthesis of steroidal 1, 2-and 1, 3-diamines as ligands for transition metal ion complexation. *Steroids* **2019**, *147*, 19–27. [CrossRef]
18. Kvasnica, M.; Budesinsky, M.; Swaczynova, J.; Pouzar, V.; Kohout, L. Platinum(II) complexes with steroidal esters of L-methionine and L-histidine: Synthesis, characterization and cytotoxic activity. *Bioorg. Med. Chem.* **2008**, *16*, 3704–3713. [CrossRef]
19. Ruiz, J.; Rodríguez, V.; Cutillas, N.; Espinosa, A.; Hannon, M.J. Novel C, N-chelate platinum (II) antitumor complexes bearing a lipophilic ethisterone pendant. *J. Inorg. Biochem.* **2011**, *105*, 525–531. [CrossRef]
20. Huxley, M.; Sanchez-Cano, C.; Browning, M.J.; Navarro-Ranninger, C.; Quiroga, A.G.; Rodger, A.; Hannon, M.J. An androgenic steroid delivery vector that imparts activity to a non-conventional platinum (II) metallo-drug. *Dalton Trans.* **2010**, *39*, 11353–11364. [CrossRef]
21. Liang, Z.; Liu, L.; Zhou, Y.; Liu, W.; Lu, Y. Research Progress on Bioactive Metal Complexes against ER-Positive Advanced Breast Cancer. *J. Med. Chem.* **2023**, *66*, 2235–2256. [CrossRef] [PubMed]
22. Koch, V.; Meschkov, A.; Feuerstein, W.; Pfeifer, J.; Fuhr, O.; Nieger, M.; Schepers, U.; Bräse, S. Synthesis, characterization, and biological properties of steroidal ruthenium (II) and iridium (III) complexes based on the androst-16-en-3-ol framework. *Inorg. Chem.* **2019**, *58*, 15917–15926. [CrossRef]
23. Lv, G.; Qiu, L.; Li, K.; Liu, Q.; Li, X.; Peng, Y.; Wang, S.; Lin, J. Enhancement of therapeutic effect in breast cancer with a steroid-conjugated ruthenium complex. *New J. Chem.* **2019**, *43*, 3419–3427. [CrossRef]
24. Khan, S.A.; Asiri, A.M. Synthesis and spectroscopic studies of Ru (II) complexes of steroidal thiosemicarbazones by multi step reaction: As anti-bacterial agents. *Steroids* **2017**, *124*, 23–28. [CrossRef]
25. Barrett, S.; De Franco, M.; Kellett, A.; Dempsey, E.; Marzano, C.; Erxleben, A.; Gandin, V.; Montagner, D. Anticancer activity, DNA binding and cell mechanistic studies of estrogen-functionalised Cu(II) complexes. *J. Biol. Inorg. Chem.* **2020**, *25*, 49–60. [CrossRef] [PubMed]
26. Huang, Y.; Kong, E.; Zhan, J.; Chen, S.; Gan, C.; Liu, Z.; Pang, L.; Cui, J. Synthesis and cytotoxic evaluation of steroidal copper (Cu (II)) complexes. *Bioinorg. Chem. Appl.* **2017**, *2017*, 4276919. [CrossRef] [PubMed]
27. Borges, L.J.H.; Bull, E.S.; Fernandes, C.; Horn, A., Jr.; Azeredo, N.F.; Resende, J.A.L.C.; Freitas, W.R.; Carvalho, E.C.Q.; Lemos, L.S.; Jerdy, H.; et al. In vitro and in vivo studies of the antineoplastic activity of copper (II) compounds against human leukemia THP-1 and murine melanoma B16-F10 cell lines. *Eur. J. Med. Chem.* **2016**, *123*, 128–140. [CrossRef]
28. Neves, A.; Verani, C.N.; de Brito, M.A.; Vencato, I.; Mangrich, A.; Oliva, G.; Souza, D.D.H.F.; Batista, A.A. Copper(II) complexes with (2-hydroxybenzyl-2-pyridylmethyl)amine–Hbpa: Syntheses, characterization and crystal structures of the ligand and $[Cu(II)(Hbpa)_2](ClO_4)_2 \cdot 2H_2O$. *Inorg. Chim. Acta* **1999**, *290*, 207–212. [CrossRef]
29. Kumar, P.; Baidya, B.; Chaturvedi, S.K.; Khan, R.H.; Manna, D.; Mondal, B. DNA binding and nuclease activity of copper(II) complexes of tridentate ligands. *Inorg. Chim. Acta* **2011**, *376*, 264–270. [CrossRef]
30. Peters, R.H.; Chao, W.-R.; Sato, B.; Shigeno, K.; Zaveri, N.T.; Tanabe, M. Steroidal oxathiazine inhibitors of estrone sulfatase. *Steroids* **2003**, *68*, 97–110. [CrossRef]

31. Prosser, K.E.; Xie, D.; Chu, A.; MacNeil, G.A.; Varju, B.R.; Kadakia, R.T.; Que, E.L.; Walsby, C.J. Copper(II) pyridyl aminophenolates: Hypoxia-selective, nucleus-targeting cytotoxins, and magnetic resonance probes. *Chem. Eur. J.* **2021**, *27*, 9839–9849. [CrossRef] [PubMed]
32. Sheoran, M.; Bhar, K.; Khan, T.A.; Sharma, A.K.; Naik, S.G. Phosphatase activity and DNA binding studies of dinuclear phenoxo-bridged zinc(II) complexes with an N,N,O-donor ligand and halide ions in a rare cis-configuration. *Polyhedron* **2017**, *129*, 82–91. [CrossRef]
33. Choi, K.-Y. Synthesis and crystal structure of phenolato-bridged dinuclear copper(II) complex with (2-hydroxybenzyl)(2-pyridylmethyl)amine. *J. Chem. Crystallogr.* **2010**, *40*, 1016–1020. [CrossRef]
34. Biswas, A.; Drew, M.G.B.; Song, Y.; Ghosh, A. Effect of anionic co-ligands on structure and magnetic coupling of bis(μ-phenoxo)-bridged dinuclear copper(II) complexes. *Inorg. Chim. Acta* **2011**, *376*, 422–427. [CrossRef]
35. Biswas, A.; Drew, M.G.B.; Gómez-García, C.J.; Ghosh, A. Use of a reduced Schiff-base ligand to prepare novel chloro-bridged chains of rare Cu(II) trinuclear complexes with mixed azido/oxo and chloro/oxo bridges. *Inorg. Chem.* **2010**, *49*, 8155–8163. [CrossRef] [PubMed]
36. Dömötör, O.; May, N.V.; Gál, G.T.; Spengler, G.; Dobrova, A.; Arion, V.B.; Enyedy, É.A. Solution Equilibrium Studies on Salicylidene Aminoguanidine Schiff Base Metal Complexes: Impact of the Hybridization with L-Proline on Stability, Redox Activity and Cytotoxicity. *Molecules* **2022**, *27*, 2044. [CrossRef]
37. Enyedy, É.A.; May, N.V.; Pape, V.F.S.; Heffeter, P.; Szakács, G.; Keppler, B.K.; Kowol, C.R. Complex formation and cytotoxicity of Triapine derivatives: A comparative solution study on the effect of the chalcogen atom and NH-methylation. *Dalton Trans.* **2020**, *49*, 16887–16902. [CrossRef]
38. Nagy, N.V.; Doorslaer, S.V.; Szabó-Plánka, T.; Rompaey, S.V.; Hamza, A.; Fülöp, F.; Tóth, G.K.; Rockenbauer, A. Copper (II)-binding ability of stereoisomeric *cis*-and *trans*-2-aminocyclohexanecarboxylic acid–l-phenylalanine dipeptides. A combined cw/pulsed EPR and DFT study. *Inorg. Chem.* **2012**, *51*, 1386–1399. [CrossRef]
39. Liu, R.-P.; Duan, M.-Y.; Li, J.; Su, Z.-P.; Zhang, J.-H.; Zhang, F.-X. Crystal structures of $[Zn(SALIMP)(CH_3CO_2)]_2$ and [Cu(SALIMP)Cl] with 2-[[(2-pyridinylmethyl) imino]methyl]phenol (HSALIMP) as a ligand. *J. Struct. Chem.* **2011**, *52*, 935–940. [CrossRef]
40. Enyedy, É.A.; Petrasheuskaya, T.V.; Kiss, M.A.; Wernitznig, D.; Wenisch, D.; Keppler, B.K.; Spengler, G.; May, N.V.; Frank, É.; Dömötör, O. Complex formation of an estrone-salicylaldehyde semicarbazone hybrid with copper(II) and gallium(III): Solution equilibria and biological activity. *J. Inorg. Biochem.* **2021**, *220*, 111468. [CrossRef]
41. Irving, H.M.; Miles, M.G.; Pettit, L.D. A study of some problems in determining the stoicheiometric proton dissociation constants of complexes by potentiometric titrations using a glass electrode. *Anal. Chim. Acta* **1967**, *38*, 475–488. [CrossRef]
42. Gans, P.; Sabatini, A.; Vacca, A. Investigation of equilibria in solution. Determination of equilibrium constants with the HYPERQUAD suite of programs. *Talanta* **1996**, *43*, 1739–1753. [CrossRef] [PubMed]
43. Zékány, L.; Nagypál, I. PSEQUAD. In *Computational Methods for the Determination of Stability Constants*; Leggett, L., Ed.; Plenum Press: New York, NY, USA, 1985; p. 291.
44. Enyedy, É.A.; Hollender, D.; Kiss, T. Lipophilicity of kinetically labile metal complexes through the example of antidiabetic Zn(II) and VO(IV) compounds. *J. Pharm. Biomed. Anal.* **2011**, *54*, 1073–1081. [CrossRef] [PubMed]
45. Rockenbauer, A.; Szabó-Plánka, T.; Árkosi, Z.; Korecz, L. A two-dimensional (magnetic field and concentration) electron paramagnetic resonance method for analysis of multispecies complex equilibrium systems. Information content of EPR spectra. *J. Am. Chem. Soc.* **2001**, *123*, 7646–7654. [CrossRef]
46. Rockenbauer, A.; Korecz, L. Automatic computer simulations of ESR spectra. *Appl. Magn. Reson.* **1996**, *10*, 29–43. [CrossRef]
47. GraphPad Prism Version 7.00 for Windows, Graph Pad Software, La Jolla, CA, USA. 2018. Available online: http://www.graphpad.com (accessed on 29 December 2023).